NANO MICRO small
www.small-journal.com

Silicon-Based Anodes for Lithium-Ion Batteries: From Fundamentals to Practical Applications

Kun Feng, Matthew Li, Wenwen Liu, Ali Ghorbani Kashkooli, Xingcheng Xiao, Mei Cai, and Zhongwei Chen**

Silicon has been intensively studied as an anode material for lithium-ion batteries (LIB) because of its exceptionally high specific capacity. However, silicon-based anode materials usually suffer from large volume change during the charge and discharge process, leading to subsequent pulverization of silicon, loss of electric contact, and continuous side reactions. These transformations cause poor cycle life and hinder the wide commercialization of silicon for LIBs. The lithiation and delithiation behaviors, and the interphase reaction mechanisms, are progressively studied and understood. Various nanostructured silicon anodes are reported to exhibit both superior specific capacity and cycle life compared to commercial carbon-based anodes. However, some practical issues with nanostructured silicon cannot be ignored, and must be addressed if it is to be widely used in commercial LIBs. This Review outlines major impactful work on silicon-based anodes, and the most recent research directions in this field, specifically, the engineering of silicon architectures, the construction of silicon-based composites, and other performance-enhancement studies including electrolytes and binders. The burgeoning research efforts in the development of practical silicon electrodes, and full-cell silicon-based LIBs are specially stressed, which are key to the successful commercialization of silicon anodes, and large-scale deployment of next-generation high energy density LIBs.

1. Introduction

1.1. Energy Situation, and Energy Storage Target

Mankind's high dependence on nonrenewable energy has led to increasing concerns on environment, climate, and human health. Meanwhile, the research and development on clean energy is becoming one of the prime topics of interest around the globe. On the one hand, clean energy from solar and wind has seen growing market size worldwide, leading to a strong demand for highly efficient energy conversion and storage devices for the wide utilization of clean energies. On the other hand, significant efforts have been devoted to the electrification of vehicles to reduce our reliance on petroleum, while correspondingly suitable energy storages devices are still under probe. Lithium-ion batteries (LIBs) have been adopted as the major energy storage technology for portable electronic devices and are also being considered for vastly different markets such as grid scale energy storage. Owing to their environmental benignity, relatively high energy density and stable performance, LIBs have found application across multiple industries. In the case of electric vehicles, the market size of LIBs can even surpass that of portable electronics. However, most EVs are not yet competent enough to replace traditional vehicles simply because of impractical driving ranges. The range from a single charge is dependent on the size/energy density of the battery. Increasing the size of the integrated battery not only increases the cost of the EV but also increases the mass of the whole electric vehicle, lowering the range. This dependence loop between cost, driving range, battery size, and total vehicle mass introduces an optimization problem and strongly depends on the system design of the EV. EVs with near practical ranges do exist in the market but the high cost from the large battery pack typically renders these too expensive. In this regard, batteries with higher energy and power density, lower cost, and improved safety are in great demand. According to the long-term goal set by the U.S. Advanced Battery Consortium LLC (USABC) to address the issue, energy density of a LIB pack system has to reach 235 Wh kg^{-1} or 500 Wh L^{-1} at a discharge rate of 1/3 C (1/3 C discharge rate indicates that a battery can be fully discharged in 3 hours),[1] in addition to the requirement of 15 years' calendar life and up to 1000 cycles. These requirements and practical needs in real applications have limited the chemistry selection of current commercially available LIBs to the marginally sufficient graphite versus lithium transition metal oxides cells. Therefore, new electrode materials and

K. Feng, M. Li, Dr. W. Liu, A. G. Kashkooli, Prof. Z. Chen
Department of Chemical Engineering
Waterloo Institute for Nanotechnology
Waterloo Institute of Sustainable Energy
University of Waterloo
200 University Ave. W, Waterloo, ON N2L 3G1, Canada
E-mail: zhwchen@uwaterloo.ca
Dr. X. Xiao, Dr. M. Cai
General Motors Global Research and Development Center
30500 Mound Road, Warren, MI 48090, USA
E-mail: xingcheng.xiao@gm.com
The ORCID identification number(s) for the author(s) of this article can be found under https://doi.org/10.1002/smll.201702737.

DOI: 10.1002/smll.201702737

chemistry that can provide drastically higher energy density and excellent cycle stability are crucial to the adaptation of next generation batteries into the EV market and beyond.

1.2. Lithium-Ion Battery Operation and Opportunities for the Battery Technology

A LIB typically consists of an anode with relatively low electrode potential versus Li^+/Li, a cathode with high potential, both of which soaked in a Li ion rich electrolyte and separated by a separator. Graphite and other carbon materials are the most widely used anode materials for LIBs due to their high abundance, low cost, stable performance in Li storage. Common cathode materials include Li metal oxides ($LiCoO_2$, $LiMn_2O_4$), and Li metal phosphates ($LiFePO_4$). Like graphite anodes, the above cathode materials also undergo reversible intercalation reactions during the charge and discharge process in LIBs. The electrolyte used in LIBs usually consists of a solution of ($LiPF_6$) dissolved in carbonate-based solvents such as a mixture of ethylene carbonate and dimethyl carbonate. Separator is a layer of Li ion permeable membrane that prevents the direct contact between anode and cathode. While the separator and electrolytes are important components of a cell, research and development in electrode materials bear significant interest because the major cost and weight of a LIB stems from the electrodes. Furthermore, the performance of a LIB is largely dominated by the quality of the electrodes. A capacity increase in anode and cathode can thus contribute to an overall increase of LIB's energy density, decrease the required mass of battery pack, and allow for the crucial wide employment of LIBs in vehicles.

1.3. Reaction Mechanisms, Challenges, and Prospects of Si Anodes

Si has received tremendous attention as an anode material because of several advantages. First, Si presents a capacity of around 4200 mA h g^{-1} upon full lithiation with the formation of $Li_{22}Si_5$. Second, Si anodes have a relatively low discharge potential plateau ≈0.4 V versus Li^+/Li of which can contribute to high working voltage when paired with a cathode, leading to a high energy density in a full LIB. Third, there is high abundance of Si element in the earth crust and the cost to obtain both single crystalline and polycrystalline Si has dropped to a range that can be accepted for electrode applications. There are other merits of Si, such as good environmental compatibility, low toxicity, and relatively stable chemical property, and all these make Si a very promising candidate for next-generation Li battery anodes.

A series of Si–Li phases exists in the process of thermal alloying of Si and Li, including crystalline phases of LiSi, $Li_{12}Si_7$, $Li_{13}Si_4$, and $Li_{22}Si_5$. These crystalline phases tend to be more kinetically stable than the corresponding amorphous phases due to their lower formation energy. However, these crystalline phases are not always favorably formed during the actual electrochemical lithiation of Si. One atomic model of crystalline Si lithiation reported by Liu et al. vividly revealed ledge peeling process the Si (111) atomic facet by Li ions.[2] Through the lattice-scale in situ transmission electron microscopy (TEM) imaging, layer-by-layer formation of Li_xSi alloy at the reaction interfaces was captured. A Si nanowire (Si NW) with a diameter of 130 nm, and a ⟨111⟩ growth direction was used for lithiation

Xingcheng Xiao is a staff scientist at General Motors Global R&D Center. He obtained his Ph.D. in Materials Science from Shanghai Institute of Ceramics, Chinese Academy of Science in 2000. He worked as a research associate at the Argonne National Laboratory and Brown University before joining General Motors in 2006. His research is focused on advanced nanostructured materials and surface sciences, with a specialization on energy-related applications.

Mei Cai is a General Motors Technical Fellow and the Manager of Energy Storage Materials Group at General Motors Global Research and Development Center. She received her M.S. and Ph.D. degree in 1993 and 1999, respectively, both in Chemical Engineering. She has the responsibility for technology innovations in the area of advanced energy storage materials development for vehicular application in General Motors. She has extensive experience in many of the energy material research areas including batteries, capacitor solar cells, hydrogen production and storage, nature gas storage, and fuel cells.

Zhongwei Chen is Canada Research Chair Professor in Advanced Materials for Clean Energy at the University of Waterloo, Waterloo, ON, Canada. He is also the Director of the Applied Nanomaterials & Clean Energy Laboratory and Director of the Collaborative Graduate Program in Nanotechnology at the University of Waterloo. He received his Ph.D. (2008) in Chemical and Environmental Engineering from the University of California Riverside. His expertise is advanced energy materials for lithium-ion/lithium–sulfur/zinc–air batteries, and fuel cells.

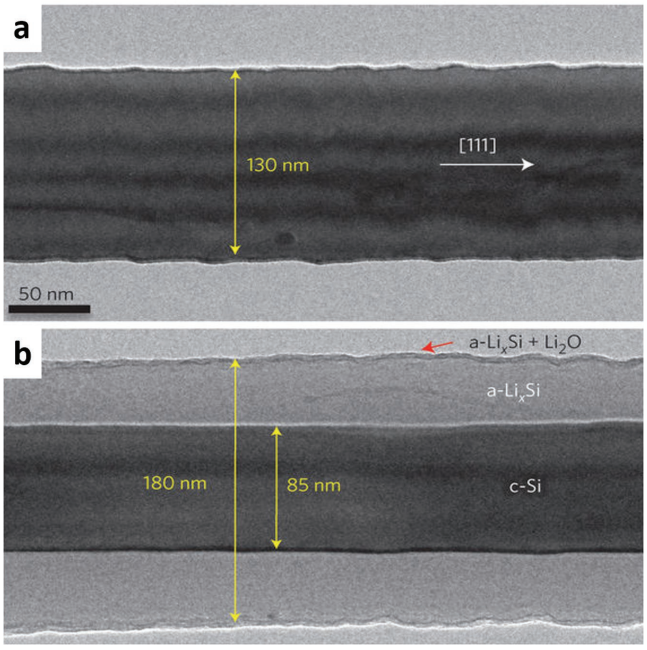

Figure 1. a) Pristine Si nanowire with rough sidewalls due to faceting, and b) partially lithiated Si nanowire with an a-Li$_x$Si layer surrounding the c-Si core. Reproduced with permission.[2] Copyright 2012, Nature Publishing Group.

(**Figure 1**a). Upon lithiation, an amorphous Li$_x$Si shell is first developed on the surface of the nanowire. Progressive migration of the sharp amorphous/crystalline interface during solid-state amorphization the Si NW is displayed in Figure 1b. The amorphous/crystalline interface has only ≈1 nm thickness with a unique contrast between the amorphous and crystalline phases. After the full lithiation of the Si NW, the volume of the wire increased by ≈280%, corresponding to a theoretical capacity of 3579 mA h g^{-1} at room temperature.

More recently, Arnaud et al. realized the mapping of elements distribution, including Li and Si by using a focused ion beam implemented in the analysis chamber of a state-of-the-art time of flight secondary ion mass spectrometer.[3] In situ focused ion beam and analysis with Auger spectroscopy effectively quantified Li concentration over the process of lithiation and delithiation at any desired cross-section site. They confirmed the core–shell progression mechanism of Li$_x$Si alloy as discussed above. Furthermore, enrichment of Li and F on the surface of Si at the beginning stage of lithiation confirmed the formation of a solid electrolyte interphase (SEI) prior to lithiation of Si. The amount of Li consumed in this process was quantified in their study. It should be noted that with the assistance of many in situ characterization techniques, such as in situ NMR,[4] in situ atomic force microscopy,[5] and in situ scanning electron microscopy (SEM),[6] the understanding of reaction mechanism of Si in LIB are becoming more approachable.

One inevitable challenge with Si anodes, as well as other alloy-type anode materials, is their poor cycling stability due to the large volume change and the resulted effects during charge and discharge. Upon full lithiation, the volume of Si can expand to more than three times of its original value. The significant volume change poses a real challenge for Si electrodes to retain its morphology over cycling. **Figure 2**a illustrates the battery performance of a bare Si electrode with an average particle size of 10 μm.[7] The electrode successfully delivers a high discharge capacity in a half cell in the first cycle with Li as counter electrode. However, irreversible capacity in the first cycle is very high (2650 mA h g^{-1}), which indicates that large amount of Li ions are irreversibly trapped in the Si electrode, or consumed in side reactions, rendering it inadequate for commercial applications. Even worse, the electrode degrades very fast and losses most of its capacity after only 10 cycles. Figure 2b–d shows a typical degradation process of a Si film electrode. Many cracks form after cycling and eventually significant amount of active material loses contact and detach from the electrode surface.[8]

In order to engineer against these problems, one must first investigate and understand the underlying natural phenomenon that is occurring. As such, a lot of previous work has been allotted to uncover the exact failure modes of Si anodes. The large volume change of Si during lithiation/delithiation causes electrode failure mainly through the following three mechanisms.

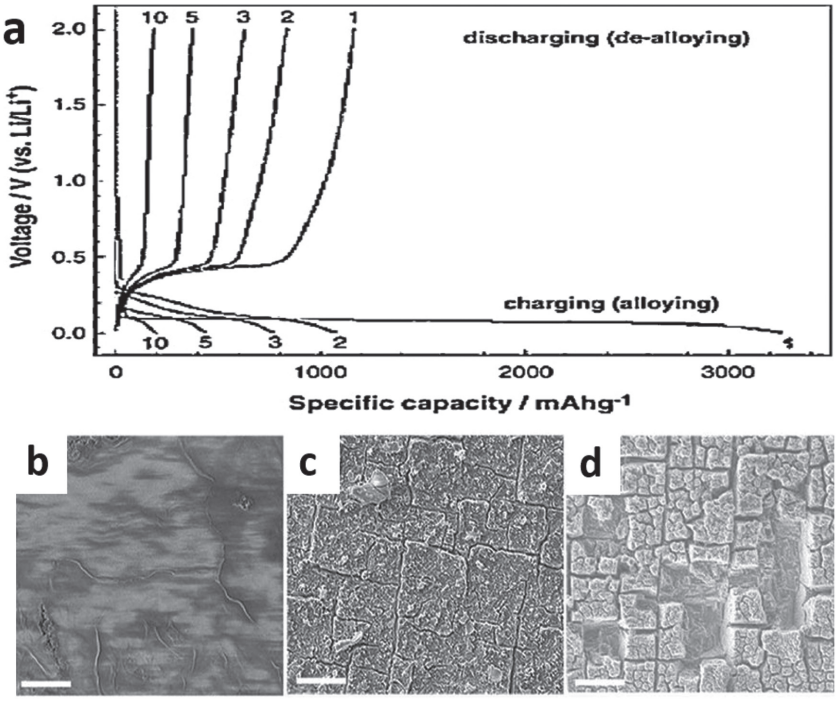

Figure 2. a) Charge and discharge profiles of a pristine micrometer-sized Si anode. Reproduced with permission.[7] Copyright 2004, The Electrochemical Society. b–d) Topview scanning electron microscope images of electrode surface morphology obtained after 3, 8, and 50 cycles, respectively. Reproduced with permission.[8] Copyright 2016, Nature Publishing Group.

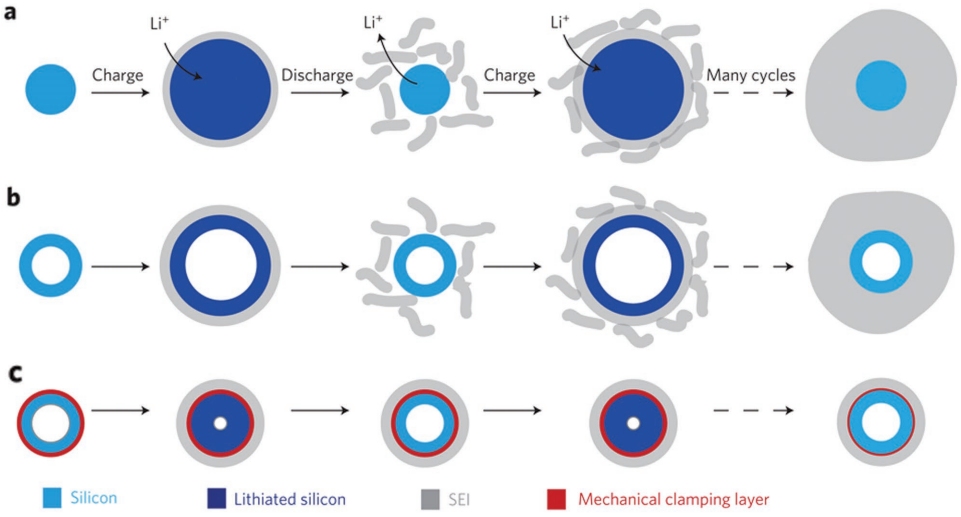

Figure 3. Schematic illustration of the lithiation process of a) solid nanowires, with repetitive SEI formation on the surface after cycling, b) Si nanotubes, with a similar outcome that SEI continues to grow upon the shrinking and expansion of the nanotubes, and c) Si nanotubes with a mechanical constraining layer on the surface, where a thin and stable SEI layer is built. Reproduced with permission.[9] Copyright 2012, Nature Publishing Group.

(1) Large volume changes in the bulky films and particles lead to high internal stress on Si, causing pulverization of Si morphology. This phenomenon is common with several other alloy-type anode materials.
(2) Upon constant volume change and pulverization, much of the active material loses electrical contact with its neighboring unit, conductive network, and current collector, and causes self-isolation of the active material and loss of electrical conductivity.
(3) Large volume changes and pulverization of Si inevitably cause the repetitive growth and formation of an unstable SEI layer as shown in **Figure 3**.[9] During the first lithiation step, electrolyte decomposes on the surface of Si anode and forms a self-passivating SEI layer. This SEI layer is majorly composed of polycarbonates, Li-based salts and oxides. It causes minimal Li-ion conduction resistance, but significantly limits electron flow. A thin passivating SEI layer can protect electrolyte from direct contact with Si and avoid further decomposition.[10] With the fracture of Si, fresh SEI continuously forms on the newly exposed Si surfaces. The formation of a stable SEI has been reported to be crucial for the long cycling of Si electrodes, however, excess continuous growth of SEI consumes significant amount of Li ions in electrolyte and further blocks electron conduction pathways deactivating Si.[11]

Apart from the electrode degeneration issues of Si, the huge volume change poses severe challenges for the design and fabrication of multistack LIBs with Si anodes as the significant volume change of Si electrode may lead to the deformation of a full cell battery. Methods such as engineering void space to accommodating the volume change usually sacrifices the volumetric energy density of Si electrodes.[12] Tremendous efforts have been devoted on different aspects to address the aforementioned issues with Si, and we will systematically review these here.

The main discussion on the research efforts on Si anodes breaks down into three parts. The development of different Si robust nanostructures is first introduced, and this includes Si nanostructures from 0D materials such as nanoparticles (NPs), hollow NPs, 1D material like nanowires, 2D film-like Si, and 3D Si structures. In addition to the quest for different robust Si nanostructures, Si has been effectively combined with various conductive or protective materials to obtain improved performance in LIBs. In this category, Si/carbon composites with amorphous carbon, carbon nanotubes (CNTs), graphene, etc., have been discussed. Structures of Si composites have also been covered. Apart from Si/carbon composites, Si/polymer composites, Si alloys, and Si/metal oxide composites are also included here. Besides all the modification and decoration on Si itself, the effectiveness of binder materials, electrolytes, and electrode designs and fabrication techniques are explored as well and have been proved to play significant roles in obtaining improved performance of Si electrodes. Research on these practical aspects not only illuminates new directions for researchers, but more importantly serves as a valuable guide for future optimization of industrial production of Si-based LIBs. In addition to the discussion of the development of Si anodes in half cells, preliminary research efforts on Si anodes adopted in full cells with commercial cathodes or the developing sulfur electrodes are also reviewed. Full-cell tests provide firsthand specific gravimetric and volumetric energy densities of Si-based LIBs, with data that are directly comparable to commercial batteries. Finally, the review will conclude with a summary and provide an outlook for the development of Si-based LIBs.

2. Robust Si Architectures: A Matter of Both Size and Structure

2.1. The Exploration of Si Nanostructures

2.1.1. 0D Si Nanostructures

Nanostructured or nanoscale Si materials have better capability in accommodating the volume change of Si due to their larger

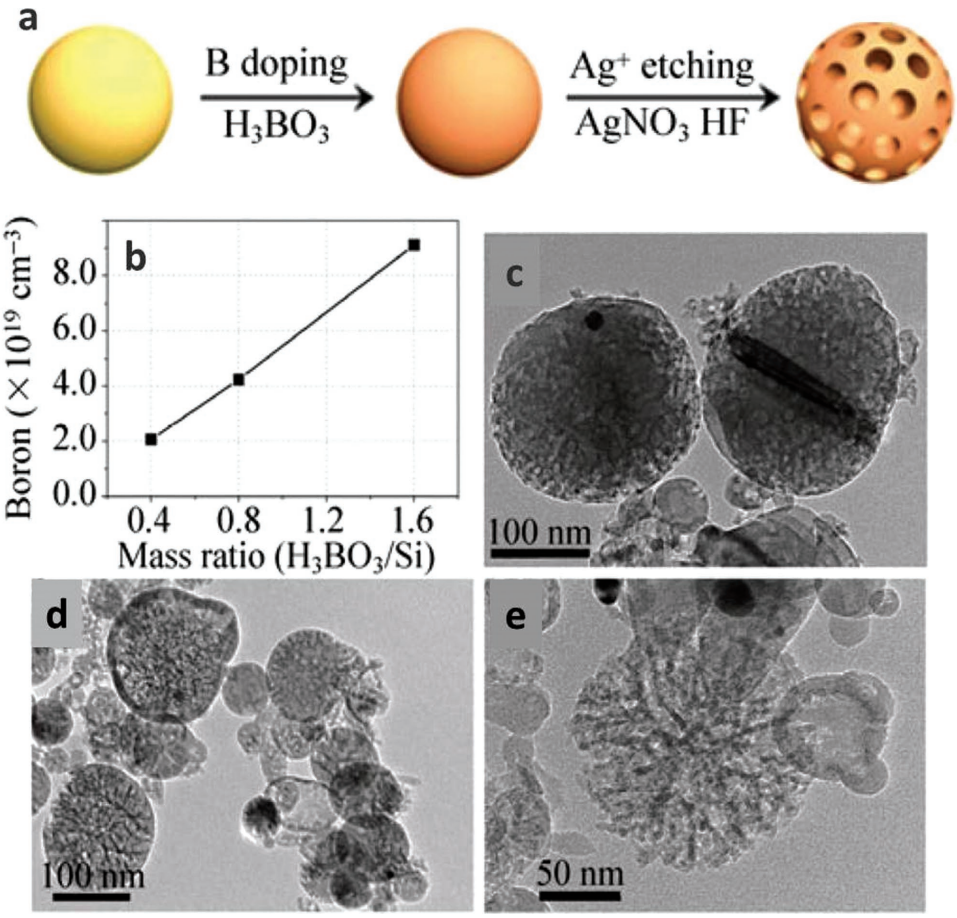

Figure 4. a) Schematic illustration of the boron doping and Ag^+ etching process, b) boron concentration versus mass ratio of boric acid to Si, and c–e) TEM images of prepared porous Si with H_3BO_3/Si mass ratios of 2:5, 4:5, and 8:5 respectively. Reproduced with permission.[20] Copyright 2013, Springer.

specific surface area and higher average binding energy per atom at the surface.[13] These materials can thus minimize the stress on them over volume change and avoid cracking or pulverization of their structures, and reduce irreversible capacity and enhance cycling stability.[14] The order of stress experienced by Si materials is also dependent on the morphology and crystallinity. On the one hand, according to the isoperimetric inequality of geometry, spheres have the least surface area compared to those in more complex shapes with the same volume. Stress on spheres are usually seen to be isotropic, while materials with higher dimensions such as Si nano thin films and NWs, have been reported to experience anisotropic volume changes due to both morphological properties and stress induced by adhesion to current collector.[15,16] In addition to changes in morphology, there have also been reports about the crystallinity and size effects of Si on the structural stability during volumetric changes. Crystalline Si transforms to amorphous Si alloy during the first lithiation process.[17] Formation of amorphous Li/Si alloy is beneficial for its mechanical stability due to the experienced isotropic mechanical stress rather than anisotropic upon volume changes.

Another commonly employed strategy is through the use of porous and hollow Si. Compared to the solid particles of Si, 0D hollow Si spheres and porous Si particles can provide better accommodation for volume change due to larger specific surface area and greater tolerance for tensile stress.[18] Yao et al. reported interconnected Si hollow nanospheres with improved cycling stability and rate performance.[19] A template of hollow silica spheres was first prepared and cast onto a stainless-steel substrate. Next, a chemical vapor deposition (CVD) process was subsequently adopted using SiH_4 at 485 °C for 20 min. Finally the silica substrate was etched away with HF. The radius of the monodisperse silica spheres or the inner radius of Si spheres was measured to be around 175 nm, and the outer radius of Si spheres was around 200 nm, with the thickness of Si being around 25 nm. The hollow Si structure delivered a specific capacity of around 2725 mA h g^{-1} for first discharge, at a rate of C/10. After 700 cycles at C/2, the material still retained a capacity of 1420 mA h g^{-1}. Ge et al. reported a doping-etching method for synthesizing nanoporous Si in the application of LIB anode.[20] As shown in **Figure 4**, commercial Si NPs were used as a starting material. Si NPs were first doped with boron, and then etched with $AgNO_3$ and HF mixed solution. The dopant content in Si increases almost linearly with the mass ratio of H_3BO_3/Si. Porous Si nanospheres were obtained after the etching process in $AgNO_3$/HF solution. Surface areas

were more than 60 m^2 g^{-1} for porous Si prepared with different dopant contents. TEM images show more porosity of Si with increasing H_3BO_3/Si mass ratios. Differential capacity was studied as a function of cell potential for the first lithiation process, and the as-obtained doped porous Si showed the peak position for initial lithiation to be 0.12 V, which is lower than that of 0.15 V for undoped pristine Si. The lowering of onset lithiation potential may a result of the increased conductivity after boron doping, shortened Li-ion diffusion path, and the reduced intercalation energy of Li ions in doped porous Si, according to the density functional theory (DFT) calculations. Both cycling stability and rate performance of porous Si were much improved over the untreated Si NPs.

Xiao et al. have synthesized hierarchically porous Si nanospheres (hp-SiNS), which consist of a porous Si shell and a hollow core.[21] In situ TEM imaging was performed throughout different states of charge and discharge to understand the lithiation/delithiation behavior of the hp-SiNS. Porous-hollow silica particles were first synthesized through simultaneous hydroxylation and condensation of octadecyltrimethoxysilane and tetraethyl orthosilicate. After removal of organic species through calcination, porous-hollow silica particles were obtained. Reduction of SiO_2 to Si with Mg was performed to obtain hp-SiNS. Possessing pores of 3.2 nm with a hollow core size of around 300 nm and an overall particle size of 400 nm the material exhibited much improved performance. With a capacity of 1200 mA h g^{-1} at C/2 and 1850 mA h g^{-1} at C/10, and more importantly, no significant capacity loss was observed. In situ TEM confirmed that during initial stages of discharge, the lithiation of the Si begins on the surface of the particle and travels inward. What is interesting is the subsequent inward volumetric expansion of the inner Si toward the center of the sphere, shrinking the hollow core. The initial expansion of the outer shell introduced a stiff Li silicide physical barrier. Lithiation of inner Si would have a preference to expand inward to relieve its mechanical stress. Therefore, with the fracturing of the lithiated Si outer shell mitigated, the surface area of active material exposed to electrolyte is kept constant, ultimately reducing the continuous SEI growth and is reflected in its excellent cycle stability.

2.1.2. 1D Si Nanostructures

The small diameter of 1D Si nanostructures largely avoids the initiation of fracture that can occur in bulk or micrometer-sized materials, and demonstrate good accommodation of stress and volume changes. In addition, 1D Si nanostructures possess good conductivity by better electrical contact between active material and conductive network or substrate, and present reduced impedance on the electrode/electrolyte interface. Widely studied 1D Si materials include Si nanowires (NWs), Si nanofibers, Si nanotubes, etc. Unlike particulate Si, which can be prepared via mechanical milling, synthesis of 1D Si structures usually requires more complex chemical process. In the application of LIBs, CVD is most commonly reported among all techniques for the fabrication of Si NWs.[22,23] Other techniques for the synthesis of 1D Si structures include molecular beam epitaxy (MBE), laser ablation, SiO evaporation, and solution-based synthesis.[24]

To the best of our knowledge, the first research on the electrochemical lithiation of Si NWs was reported by Zhou et al. in 1999.[25] Another research paper was published by the same group in 2000, and these Si NWs were first adopted as a LIB anode material.[26] In the subsequent few years, there were only several papers discussing the 1D Si materials in the application of LIBs.[27] Thus far, majority of the research on 1D Si materials was still focused on their lithiation behaviors, or doping effects. Although vapor–liquid–solid (VLS) mechanism was proposed for the synthesis of Si NWs decades ago, 1D Si materials reported in LIBs were mainly prepared via laser ablation, or lithography. More recent research on Si NWs in LIBs did not appear until 2008, when two groups almost concurrently researched their electrochemical properties in LIBs, both of the work using Si NWs synthesized via VLS mechanism.[23,28] Chan et al. conducted a comprehensive study of the challenges with bulky Si film and particles, and exhibited advantages of nanowire morphology for Si in the application of LIB anodes. The authors designed a directly grown, binder-free, and conductive-additive-free Si electrode. Si NWs were grown on the stainless steel substrate using SiH_4 as Si precursor and Au as a catalyst. The reaction was conducted at a temperature of 530 °C with pressure of 30 Torr in a CVD chamber. The reported Si NW electrode can provide enough space for volume expansion, and the nanowires have good capability in relaxing stress induced from volume change. Direct growth of the nanowires also ensures the good electrical conductivity between the active material and the current collector. The authors reported an initial specific capacity of 4277 mA h g^{-1} for lithiation, allegedly equivalent to the theoretical capacity within the range of experimental error. The subsequent delithiation presented a specific capacity of 3124 mA h g^{-1}, both of the values higher than previously reported. The lithiation capacity was stabilized at around 3500 mA h g^{-1} for 20 cycles at a rate of C/5. Unlike Si films with thickness greater than 2 μm, Si NWs do not show the recrystallization process during deep discharge to 20 mV.[29] This also resonates with our discussion above that nanostructured Si facilitates isotropic stress relaxation during lithiation and delithiation processes. The significance of Chan's work not only lies in the discovery of performance increase by 1D Si, but also sheds light on the exploration of more sophisticated Si structures. Ever since, there have been intensive studies on developing Si anodes based on Si NWs and other Si nanostructures with advantages in various aspects, as well as on the lithiation mechanism.[22,30]

Si nanofibers, another type of 1D Si materials, are mostly produced via spinning, including electrospinning methods, or prepared with the support of a fiber substrate.[31,32] Lee et al. reported a LIB anode using electrospun 3D mesoporous Si nanofibers, in which primary Si NPs interconnected and formed a secondary mesoporous fiber structure, with enhanced electron and Li^+ diffusion compared to Si NPs.[33] A soft Si anode was realized by Xiao et al. with a flexible composite of Si/Ni/polyvinylidenefluoride (PVDF) fiber.[34] As shown in **Figure 5**, a PVDF membrane was fabricated via an electrospinning process, and used as the backbone for the subsequent Ni deposition and Si coating. Although the polymer substrate provided

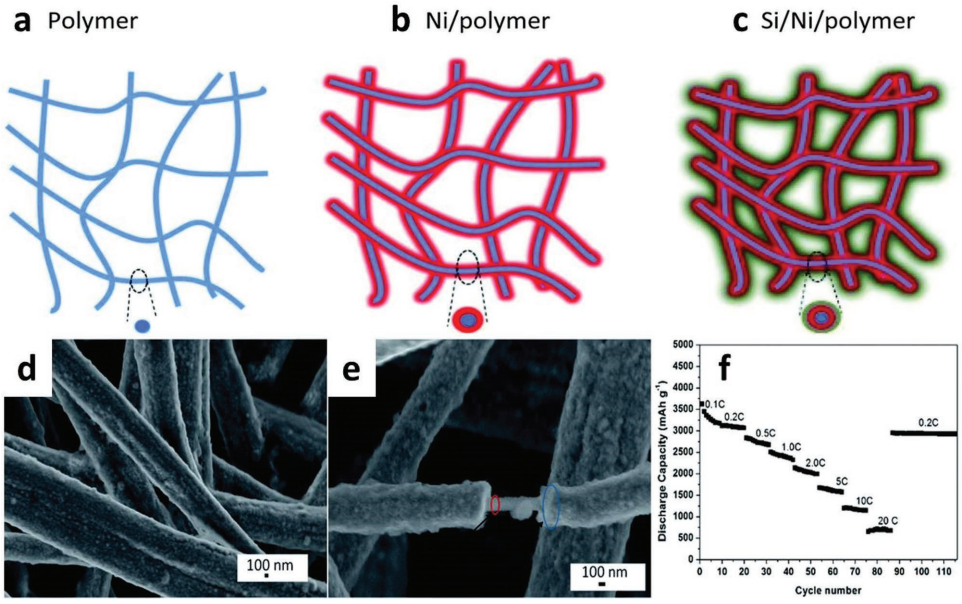

Figure 5. Schematic drawings of a) polymer substrate, b) polymer substrate with electroless-deposited Ni, c) Si coating on the coaxial Ni/polymer substrate, d) SEM image of Si/Ni/Polymer coaxial nanofibers after 200 cycles, e) a cross-section view of Si/Ni/polymer nanofiber after 200 cycles, and f) cycling performance of the composite with charge and discharge rates from 0.1 to 20 C. Reproduced with permission.[34] Copyright 2014, Royal Society of Chemistry.

good flexibility and robustness, it was however not electrically conductive. The deposition of a thin Ni layer transformed the nonconductive polymer into a conductive network. Thus far, a coaxial Ni/PVDF nanofiber network was prepared and ready to be used as the substrate for Si coating as well as the current collector. Amorphous Si was coated on the fiber substrate using a radio-frequency (RF) magnetron sputtering technique. It is interesting to note that the structure of the Si/Ni/PVDF coaxial nanofiber maintained good stability, the surface of Si remained mostly intact, and most of Si coating firmly attached to the PVDF backbone after 200 cycles (Figure 5d,e). This provided insight into the benefits of this system and could explain the good electrochemical performance, shown in Figure 5f. Various charge and discharge rates were applied, and the electrode was electrochemically stable at high rates such as 10 and 20 C.

Si nanotubes have recently aroused a lot of research interests in the application of LIB anodes due to their unique 1D hollow structure.[9,35–37] Compared to Si NWs and nanofibers, Si nanotubes usually bear a much higher specific surface area due to their hollow structure. Park et al. attributed the high rate performance of their Si nanotube anode to the high surface area of Si nanotubes. A larger Si/electrolyte interface allows the Li insertion to take place from both the inner and outer wall of the nanotubes.[37] In addition, the hollow space inside the tubes can play a significant role in maintaining the structure of Si, because the stress from volume change are now allowed to be released both inward and outward. The macroscopic volume change of the Si nanotube electrode can be controlled to be much less than that of regular Si structures, which expand around 300% at full lithiation. Interestingly, Song et al. managed to investigate and elucidate the underlying principles for the improved electrochemical performance of Si nanotubes.[35] Two major considerations were taken during the modeling. First was isotropic expansion of Si associated with Li insertion (stress free), while the second was the expansion from stresses (i.e., misfit stresses) that were caused by the filling of vacancies between Si atoms by Li atoms.[38] The changes in radial and axial aspects were derived and expressed in the following equation

$$\frac{\mathrm{d}R_{\mathrm{out}}}{R_{\mathrm{out}}}-\frac{\mathrm{d}h}{h}=\frac{3(1+\nu)\sigma^{*}}{E\left(R_{\mathrm{out}}^{2}-R_{\mathrm{in}}^{2}\right)}\int_{R_{\mathrm{in}}}^{R_{\mathrm{out}}}\left[\frac{1-\lambda(r)}{2+\lambda(r)}\left(1-\frac{R_{\mathrm{in}}^{2}}{r^{2}}\right)\right]r\,\mathrm{d}r \qquad (1)$$

In this equation, R_{out}, R_{in}, and h are the outer radius, inner radius, and the height of the nanotubes respectively. E and ν stand for Young's modulus and Poisson's ratio of the material. σ^{*} is the misfit stress inside the alloy, and λ is the function of the misfit distribution. Equation (1) can be adapted to describe the expansion behavior of Si NWs by simply taking R_{in} as 0.

2.1.3. 2D Si Nanostructures

Si thin films have received much attention in the application of LIB anodes due to the much improved electrochemical performance, as well as their simple electrode configuration.[39] The research of Si thin films in LIBs can be dated back to early 2000s.[29,40,41]

In general, Si thin films can be prepared by two common techniques: CVD and physical vapor deposition (PVD). Similar to the synthetic process of Si NWs, gaseous Si-containing precursors decompose in a CVD chamber at elevated temperatures between 500 and 1000 °C, with the presence of a catalytic substrate. In the application of LIBs, common catalytic substrates include stainless steel, Cu, Ni, or Ti. Si thin films prepared

via CVD usually have polycrystalline structures. PVD, a term commonly is known to describe various vacuum deposition methods for the fabrication of not only Si but also a whole repertoire of thin-film materials. The Si precursors for PVD can have very high purity or can be purposely doped according to the final application.[42]

Ohara et al. examined an n-type Si thin film deposited on Ni foil in LIBs, and observed extremely high capacity and long cycle life.[40] The authors found n-type Si film outperformed the intrinsic Si and the p-type Si films in terms of capacity and cycling stability. Three thicknesses were examined, including 500, 1000, and 1500 Å. The 500 Å film delivered the highest specific capacity and the best durability, achieving a reversible capacity of ≈3800 and 3600 mA h g^{-1} at 1 and 2 C, respectively, after 200 cycles. The 500 Å thick n-doped Si film also showed great rate performance. The electrode was able to deliver a specific capacity of around 3000 mA h g^{-1} after 1000 cycles at 12 C, which corresponded to a charge/discharge time of around 5 min. In this case, the superior performance was largely explained by the excellent conductivity of the electrode due to its thin structure. One should note that while literature demonstrated a promising example of Si thin film for LIB anodes, the commercial LIB electrodes usually bore an areal capacity of 1.5–2 mA h cm^{-2}, which required the thickness of Si thin films to be a few micrometers. The problem of Si areal mass loading had as expected, posed a detrimental challenge for the practical application of Si thin films in commercial LIBs.

2.2. The Resurrection of Micrometer-Sized Si and Si-Based Structures

Despite the unique benefits of nanosized Si, the inevitable disadvantages such as low tap/pressing density, low Coulombic efficiency (CE), and complex synthesis have hindered its wide applications.[43] Hence, it is meaningful and practical to engineer micrometer-sized structures, with characteristics of nanosized Si. This approach cannot only retain the advantages of nanosized Si, but also eliminate the associated drawbacks of it. The lithiation and electrochemical behavior of micrometer-sized Si was studied in 1990s and early 2000s, prior to the wide-spread research efforts on various Si nanostructures.[44] However, the intrinsic properties of Si had limited the development of micro-sized Si. Some significant breakthroughs with micrometer-sized Si were later achieved, largely due to the successful development of various Si nanostructures.

In general, there are two methodologies for the design of micrometer-sized Si with improved cycling performance in a LIB. One is the engineering of 3D structures of Si, with nanocharacteristics, such as nanopores, nanograins.[45] The other methodology is to incorporate nanosized Si onto a micrometer-sized host, such as graphite, and various carbon frameworks.[46–48]

3D Si-based anode materials are of great interest as they can absorb the advantages of nanostructures from 0D to 2D, while extend these merits to a 3D scale. The inherent features of nanostructures such as nanosized Si, nanopores on both Si structures and Si composites, can help avoid Si pulverization due to repetitive charge and discharge. In addition, these features can also provide necessary space for volume change to maintain the electrode integrity, and facilitate electrolyte diffusion inside the 3D structures.

In 2008, Kim et al. developed a 3D carbon-coated Si electrode from bulk Si particles.[49] The macroscopical morphology of the bulk Si precursor well maintained its morphology after the pore-generating process, with sizes of which ranged from a few to near 100 μm. Plenty of nanosized "octopus-foot-like" voids were created, with thickness of Si walls being around 40 nm (**Figure 6**a). The specific surface area of the 3D c-Si reached 158 m^2 g^{-1}, proving its high porosity. As one of the earliest researches probing the nanomorphologies of Si anode materials, the 3D c-Si electrode displayed very compelling cycle performance. The electrode showed an initial capacity of above 2800 mA h g^{-1}, and retained over 99% of its capacity after 100 cycles at 0.2 C. When a higher current of 1 C was applied, the electrode successfully retained 90% of its original capacity. These capacity retentions were superior to all previous reports with Si anodes, which stemmed from the benefits from both 3D Si nanowalls and large number of nanopores. More recently, Yi et al. have successfully synthesized micrometer-sized Si, with an interconnected structure of Si and carbon, using SiO as the starting material (Figure 6b).[50] The Si–C composite exhibits an reversible capacity of 1675 mA h g^{-1} at 400 mA g^{-1} and has 96.6% capacity retention after 50 cycles. The Si–C electrode maintains high specific capacities of 1100 and 700 mA h g^{-1} at high currents of 6.4 and 12.8 A g^{-1}, respectively (Figure 6c). This excellent performance can be explained by the nanoscale nature of Si and carbon building blocks. The interconnected Si–C network at micrometer scale can ensure good structural integrity and electrical conductivity.

In addition to the engineering of micrometer-sized Si with nanofeatures, the incorporation of nano-Si onto a micrometer host is a more universal approach, and has obtained fruitful achievements.[51,52]

Graphite, the current mainstream anode material, has been the dominant anode material throughout commercial LIBs' history. Good cycling stability, low cost, and a few other merits have granted graphite its current status. It is therefore highly desirable for Si-based anodes to retain these merits while maintaining its high capacity for Li ions in order for Si to secure its presence in the anode market. A combination of Si and graphite is a realistic way to obtain the desired stable anode, with proper balancing between the loading amount of graphite and Si, and careful engineering. Efforts on the combination of Si and graphite can be dated back to the beginning of 21st century, when most of the Si/graphite composites were prepared via mechanical mixing, such as grinding or ball milling.[53] Remarkable capacity increase has been observed with these composites. However, mechanical mixing inevitably introduces structural damages to graphite, which deteriorates the stability of SEI formed on the surface of graphite and leads to quick deterioration of the electrode. In addition, the unbound Si particles in this type of electrodes can easily lose their connections with the conductive network due to volume change and the repetitive growth of SEI. Thus, it is critical to tailor the morphology, and the ratio of Si in the composite to maximize the benefits of the combination of Si and graphite.

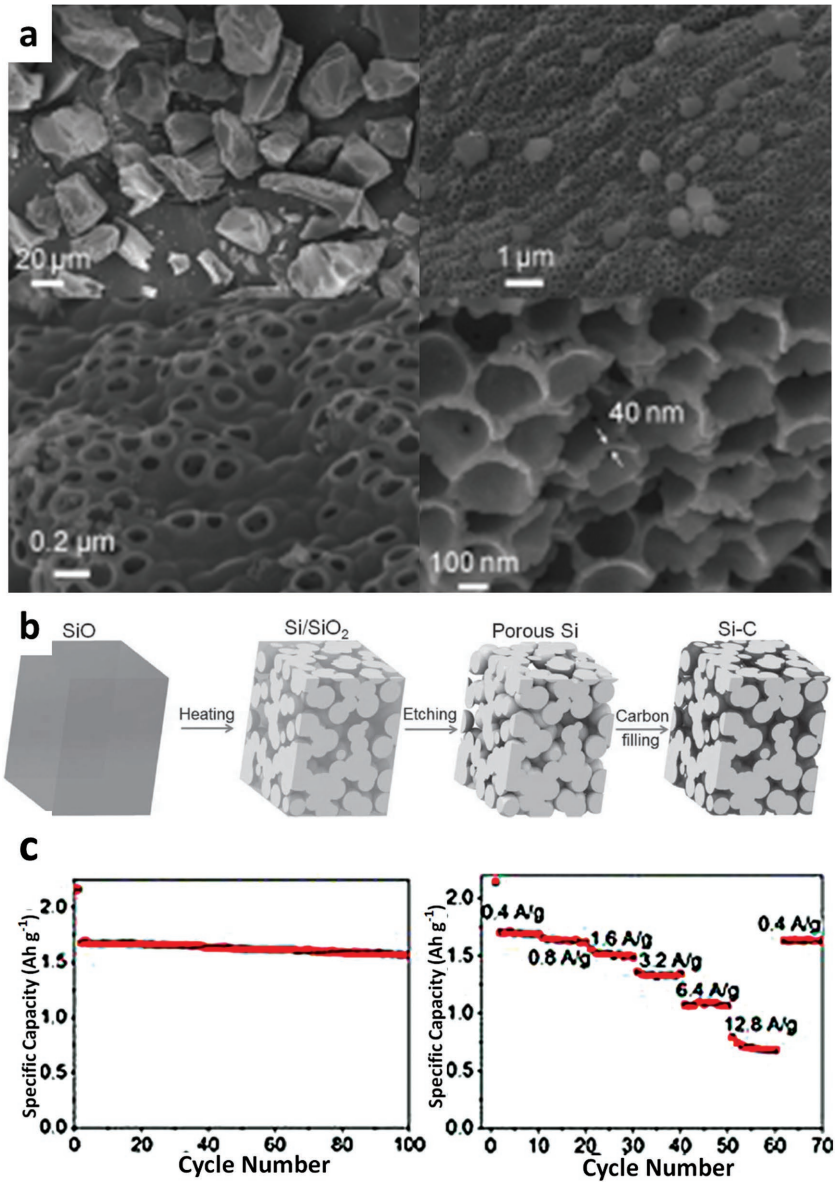

Figure 6. a) SEM images of 3D porous Si–C particles at different magnifications. Reproduced with permission.[49] Copyright 2008, Wiley-VCH. b) Schematic drawing of the synthetic procedure of micrometer-sized interconnected Si–C structure. c) Cycling performance of Si–C electrodes at 400 mA g^{-1}, and multiple rates. Reproduced with permission.[50] Copyright 2013, Wiley-VCH.

Ko et al. have developed a scalable method for the synthesis of silicon-nanolayer-embedded-graphite (SGC) based on commercial graphite.[54] In their work, Si nanolayer was uniformly grown on both the surface, and the internal pores of graphite via a CVD process (**Figure 7**a). The subsequent carbon coating generates a thin carbon layer on Si surface (Figure 7b,c). The Si nanolayer, distributed throughout the graphite particles and internal pores, significantly contributes to the capacity increase of the composite. Meanwhile, the nanosize nature of the Si layer can not only effectively accommodate the induced stress during lithiation and delithiation, but also provide fast Li-ion transport without creating significant hindrance on the diffusion of Li to graphite. The thin-layer C coating on Si improves the electric and ionic conductivity of the composite, and facilitates the stable formation of SEI. When the Si content was manipulated to be 6% in weight in the SGC composite, the reversible specific capacity reached 517 mA h g^{-1}, with a very high initial CE of 92%, identical to that of the raw graphite used in this work. In addition, the cycling stability of the composite electrode resembled that of the graphite anode, confirming Si's commercial relevancy in terms of both superior capacity and cycling stability. It is also important to note that a full-cell LIB of this composite with $LiCoO_2$ as cathode was fabricated. The areal capacity the SGC anode was controlled to be 3.3 mA h cm^{-2}, slightly higher than that of the commercial $LiCoO_2$ cathode (Figure 7d). The stability of the $LiCoO_2$/SGC cell was comparable to that of the $LiCoO_2$/G cell, at various rates up to 3C (Figure 7e). 92% capacity retention was achieved after 100 cycles. Minor deformation on the charge/discharge profile can be observed at both increased rates and extended cycles (Figure 7f,g), confirming the stable nature of the SGC electrode. More impressively, energy density of the full-cell device was calculated to be 1043 Wh L^{-1}, and the average voltage was around 3.77 V. In virtue of the above-mentioned benefits, this SGC composite has demonstrated a potentially applicable approach to increase the capacity of current graphite anode by combining with Si while taking electrochemical performance, actual battery design, and scalable production into consideration.

Another approach of interest is to integrate nanosized Si with micrometer-sized carbon frameworks. In this approach, Si can be well distributed in the secondary structure, and the embedding of Si is usually accomplished simultaneously with the formation of micrometer-sized Si composite. The accessory materials and the reaction conditions can be easily controlled to tune the morphology of secondary particles. Specific surface area of the material can be reduced to favor the formation of a stable SEI. It is desirable to tailor appropriate voids inside the micrometer particles to function as buffer zone for Si volume change, maintaining the robust structure and conductive network. Compared to pure Si nanostructures, secondary micrometer-sized Si structures usually present a higher tap density, which is a crucial factor in the design of practical LIBs. Methods for the fabrication of micrometer-sized Si structures include spray-dry,[52] nebulized-spray-pyrolysis,[47] CVD,[55] etc., and the raw material selection for the formation of carbon frameworks can also be broad.

Xu et al. reported a type of watermelon-inspired Si/C microspheres, in which hierarchical buffer structure and optimized

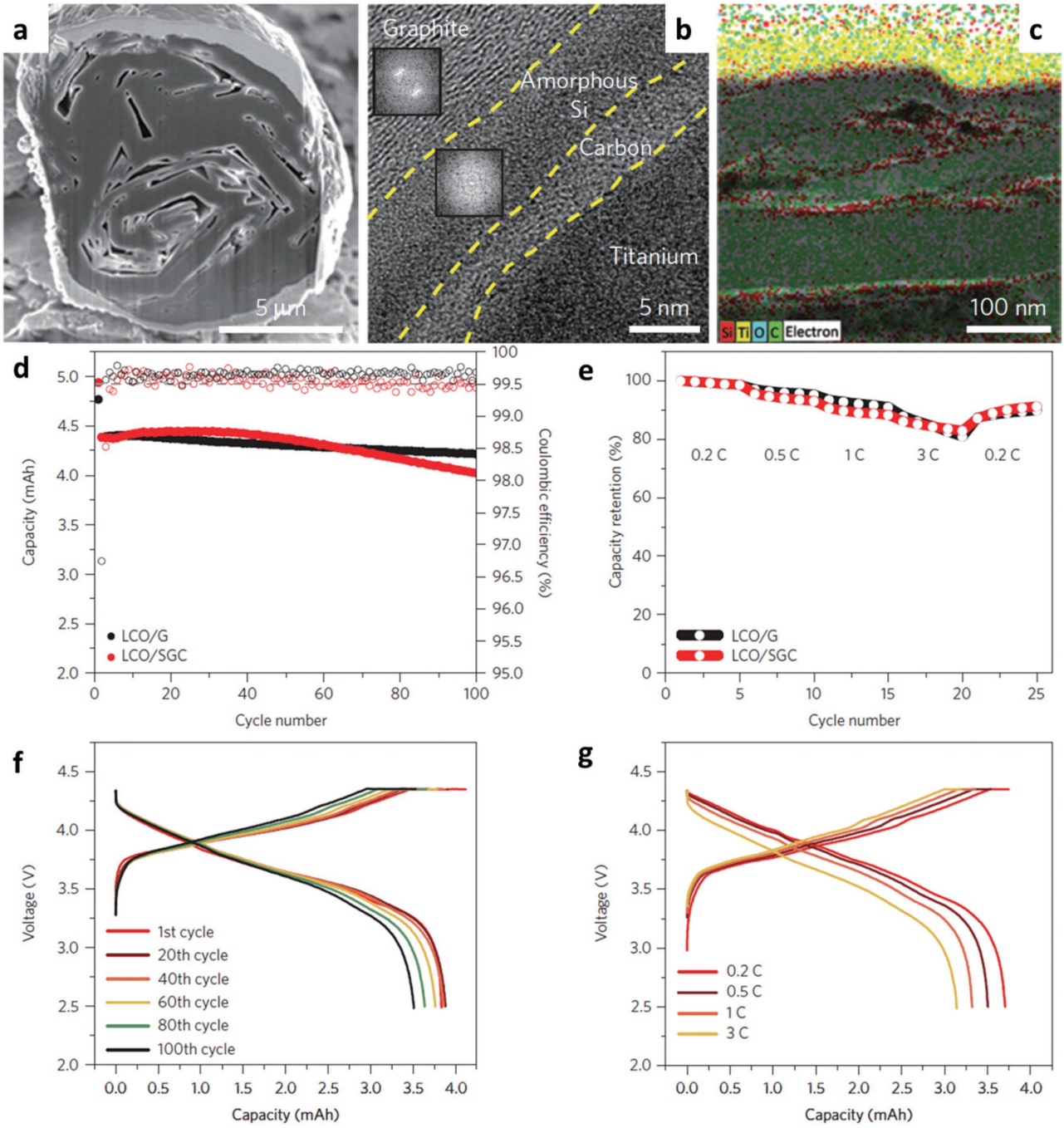

Figure 7. a) SEM image of cross-section SGC composite. b) HR-TEM image at the interfacial region of the SGC composite, with fast Fourier transform images inset at specific regions. c) STEM images for elemental mapping by energy-dispersive spectroscopy. d) Cycle performance of $LiCoO_2$/G and $LiCoO_2$/SGC composites at a charge rate of 0.5 C and discharge rate of 1 C, respectively, in a potential window of 2.5–4.35 V. e) Rate capability tests of $LiCoO_2$/G and $LiCoO_2$/SGC batteries at various discharge rates from 0.2 to 3 C. f) Charge/discharge profiles of $LiCoO_2$/SGC of different cycles. g) Charge/discharge profiles of $LiCoO_2$/SGC at different rates. Adapted with permission.[54] Copyright 2016, Nature Publishing Group.

size distribution were reportedly carefully designed and tuned.[56] As illustrated in the schematic in **Figure 8**a–c, Si NPs with carbon coating were evenly distributed in the matrix of flake graphite, and another layer of carbon deposition was conducted to prevent the loosening of the microspheres and further increase the tap density of the spheres. The size variation among particles can reduce dead space in between particles and can be beneficial to dense packing. The tap density of the as-prepared Si/C microspheres was measured to be 0.88 g cm^{-3}, much higher than that of the nano-Si particles (0.21 g cm^{-3}), and this is of great significance in the construction of densely packed electrodes. The mass loading

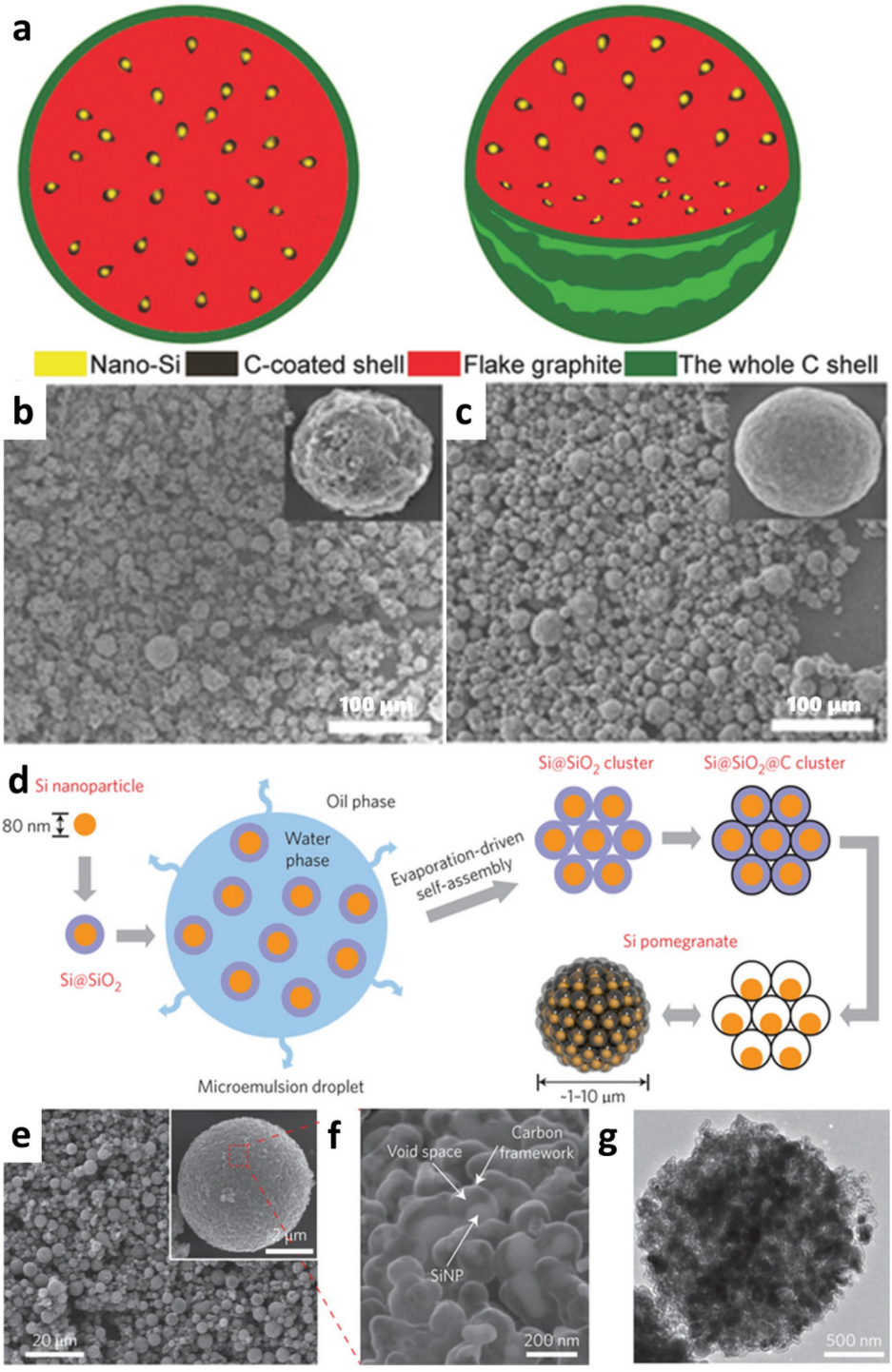

Figure 8. a) Schematic illustration of the watermelon-inspired Si/C microspheres, Si/C b) before, and c) after the carbon coating process. Reproduced with permission.[56] Copyright 2016, Wiley-VCH. d) Schematic of the fabrication process for Si pomegranates, e–g) low-magnification, high-magnification SEM images, and TEM image of Si pomegranates. Reproduced with permission.[57] Copyright 2014, Nature Publishing Group.

of Si/C microspheres reached 4.1 mg cm^{-2}, contributing to an areal capacity of 2.54 mA h cm^{-2}. It is interesting to note that the initial CE of this material reached 89.3%, which the authors attributed to the hierarchical structure of Si/C microsphere that allows full penetration of electrolyte, and the good electronic and ionic transport in the carbon-based framework.

Liu et al. constructed a pomegranate-like structure with carefully tailored conductive carbon framework and internal void between Si and carbon.[57] As shown in Figure 8d–g, a layer of

SiO_2 was deliberately coated on the surface of Si NPs, before the resorcinol-formaldehyde polymerization and the subsequent carbonization of polymer coating. HF was later used to remove the SiO_2 layer and create the desired void space that can accommodate the volume change of Si during charge and discharge process. The secondary particles have a good spherical shape and the diameter ranges from 0.5 to 5 µm. Si NPs, carbon framework, and the well-defined voids can be clearly observed in the SEM and TEM microscopic images. An increase of tap density from 0.15 to 0.53 g cm^{-3} was achieved with the formation of the secondary pomegranate structure from Si NPs. The authors reported a high volumetric capacity of 1270 mA h cm^{-3} of the Si pomegranate electrode, which is twice that of commercial graphite anodes. Extra-long cycling of the electrode was also displayed with 97% capacity retention after 1000 cycles.

3. Versatile Si-Based Composites

Apart from the quests for different morphologies of Si, Si-based composites are another focus for the development of high-performance Si anodes. Si-based composites have been widely studied to overcome the difficulties of Si anodes resulting from the intrinsic properties of Si. As previously discussed, notorious issues with Si anodes arises from the significant volume changes, including electrode structure degradation, loss of contact points between active material and conductive network, and unstable SEI formation. It is impossible to tackle all these issues by solely engineering Si morphologies. Different carbon-based conductive additives have proven to be essential for the electrode conductivity improvements in LIB electrodes and as a result, the electrochemical performance of electrode. These conductive materials have also been found to be vital for the improvement of Si electrodes, not only by the enhancement of the electrical conductivity of Si electrodes, but also in some cases, buffering the volume change of Si during lithiation process, and stabilizing the SEI. Thanks to the size effect of nanomaterials, nanosized Si anodes have shown significant improvement over micrometer-sized Si. With the presence of conductive additives in the slurry composition, these nanosized Si achieved further improvements, benefiting from better electrical conductivity and accommodation for volume change.[58] In 1999, Li et al. used laser-induced silane gas reaction and prepared pure nanoscale Si powder with a mean diameter of 78 nm. They presented a capacity of around 1400 mA h g^{-1} after 20 cycles with their Si electrode that contained 40% Si, 40% carbon black, and 20% PVDF binder.[59] However, simple addition of conductive agents cannot provide an intact and robust matrix protecting Si and stabilizing SEI, and thus the performance improvement is limited. Tremendous efforts have been made to create more efficient conductive and protective networks. The opportunity for using composite materials can allow the research community to imagine quite creative designs, achieving high performance while providing valuable insight on key mechanisms. By dwelling into these novel avenues of thought, a simple and elegant design could arise sometime in the near future and the long-sought-after Si anode will finally become a viable commercial reality. In the following sections, this review will provide a comprehensive overview of the work that has been done on a variety of Si composites, including various Si/C composites,[60,61] Si/graphene[62,63] and Si/CNT composites,[64,65] Si/conductive polymers,[66] Si alloys[67,68] and Si/metal oxide composites,[69] etc.

3.1. Simple Si/C Composites, Si/C Core–Shell and Yolk–Shell Composites

Before the thriving of research on various Si morphologies, the combinations of Si particles with carbonaceous materials were found to be an effective approach to improve Si anodes. A carbon-based matrix support can not only provide a conductive network for the Si active material, but also accommodate the mechanical stress of the active phase over the up-take and release of Li in Si. One widely used method for the mixing of Si and carbon materials is high-energy ball milling, in which Si and carbon precursors are milled in a jar filled with inert gas. Solution-based mixing is another commonly used method for the construction of Si/C composites. A pyrolysis step is usually followed to carbonize the carbon-containing micro molecules or polymers.[70] Si et al. studied the effects of both the size of Si particles and the precursor polymers on the electrochemical performance of their Si/C composites.[71] The size of Si particles included 10 µm, 4 µm, 0.7 µm, and 50 nm. Polyvinyl chloride (PVC) or chlorinated polyethylene mixed with Si was thermally decomposed into carbon and formed a Si/C composite. The variation of chlorine content in the polymers largely affected the yield of carbon, thus their structure and physical properties after pyrolysis. These composites with nanosized Si outperformed the composites with bigger Si particles. Chlorine content in polymers and the ratio of polymer in Si/polymer mixtures were both found to be effective in affecting the electrode performance. Takeda et al. aimed at finding a suitable precursor for the pyrolyzed Si/C composites, and they found the fluorine-containing precursors have a substantial improvement over the bare nano-Si particles.[72] In their study, Si/C composite with PVDF-generated carbon showed significant improvement in stability over bare Si NPs. In addition, the CE of the Si/C composite was increased to 75% compared to 66% of the bare Si NPs. More interestingly, there was also an increase of the capacity retention rate over other commonly used carbon sources including PVC, pitch, sucrose, etc.

Beyond the improvement of Si anodes by addition of carbon via simple mixing or pyrolysis of carbon precursors, Si/carbon composites have been advanced with more delicate core–shell design, and the introduction of void space in between Si and carbon. The Si/C core–shell design was first proposed and realized in order to solve the electrical conductivity issue, and the repetitive SEI growth on the surface of Si. Jung et al. demonstrated a Si/C composite via the carbonization of resorcinol formaldehyde on the surface of Si NPs.[73] They attributed the improved cycling stability to the stable conductive network arising from the enhanced contact between Si and coated carbon. SEI formation on the surface of Si was briefly mentioned, without much stress on its effect. Authors also observed cracks on carbon shell, which might be a plausible cause for the capacity decay, however, no solution was provided. Additional work has been reported on core–shell

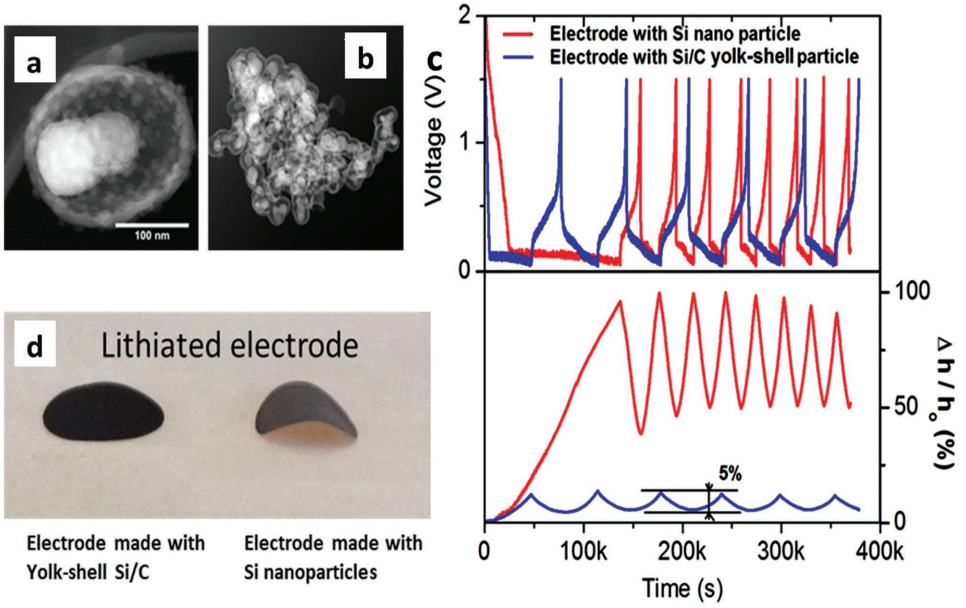

Figure 9. TEM images of a) single Si/C, and b) associated Si/C yolk–shell structure. c) Comparison of charge and discharge profiles, and electrode thickness fluctuations between bare Si electrode and yolk–shell Si/C electrode. d) A picture of lithiated yolk–shell Si/C electrode and bare Si electrode. Reproduced with permission.[79] Copyright 2015, Wiley-VCH.

Si/C composites, with modified methodologies and synthetic routes.[60,74] Various Si morphologies have been adopted in the design of core–shell Si/C composites, combining the advantage of both versatile Si morphologies and the core–shell structures.[31,75,76]

Due to the significant volume change of Si during Li insertion and extraction process, rigid Si composites usually tend to lose their structural integrity over cycles. Stress generated from Si expansion leads to the breakdown of surface coating layer, and the detachment of Si from the conductive network. Furthermore, the constant volume change detaches any SEI layer formed on the surface of Si, this leads to constant generation of electrically insulating material which over many cycles can significantly increase the resistance in the electrode. Hence, the void space in between the carbon shell and the Si core in a Si/C composite is critical in maintaining the composite morphology and to stabilize the SEI on the surface of the composite over cycling. In addition, to avoid excess isolation of Si from Li^+ in electrolyte by the carbon shell, consideration has been given to the creation of pores on the carbon shell.[77] Li et al. reported a hollow core–shell structured Si/C composite for LIB anode in 2012, intentionally introduced void space between Si core and carbon shell by etching away SiO_2 from the surface of Si NPs precursor.[76] Shortly after that, Liu et al. first used the term "yolk–shell" for their alloy-type anodes, in which Si/C composite displayed a high specific capacity of around 1500 mA h g^{-1} at 1 C, and excellent durability, with 75% capacity retention after 1000 cycles.[78] Carbon coating over Si was largely reserved after cycling, and volume expansion of Si was less disruptive to the conductive network compared to core–shell Si/C composites without void space. A stable and thin SEI was observed on the surface of carbon, owing to the rigid carbon shell that minimized the volume change effect of Si on the SEI and limited direct contact between Si and electrolyte.

Investigating deeper into the mechanism of coated Si composites, Xiao et al. first demonstrated that the york–shell structure could effectively suppress the breathing effect of Si electrode.[79] In situ TEM images in **Figure 9**a,b vividly illustrated the yolk–shell morphology, in which free space was created between C shell and Si NP. This design can accommodate the significant stress from Si volume expansion and contraction during the charge and discharge process. In addition, the majority of SEI will form on C shell, which has much less expansion comparing with Si. As a result, the SEI layer can be stabilized and leads to high cycle efficiency. Figure 9c compares both the charge and discharge profiles, and the electrode thickness changes between regular Si NP electrode and yolk–shell Si/C electrode over cycling time. Their in situ electrochemical dilatometer results show that the thickness of Si NPs based electrode has about 40% irreversible expansion and then 50% reversible changes during the charge and discharge. The large thickness change would cause the movement of battery tabs and eventually cause the failure of the battery pack. In contrast, with the yolk–shell structure, the electrode thickness can be suppressed down to 5%, which meets the requirement of battery pack design. The stress induced from lithiation can also be reduced as evidenced by Figure 9d.

To further explore the merits of voids and pores in Si/C composites, Yang et al. designed a yolk–shell Si mesoporous carbon composite, in which both voids and pores are carefully tailored.[77] In their work, Si NPs were first encapsulated by a solid SiO_2 layer, followed by the coating of another porous SiO_2 template for C growth via the pyrolysis of phenolic resin precursor at high temperature. Both the SiO_2 layers were subsequently removed by HF etching, leaving void space in between Si and C, and abundant pores on the carbon shell. The authors have taken the advantages of several key features of the composite. Nano-sized Si active material prevents the electrode from

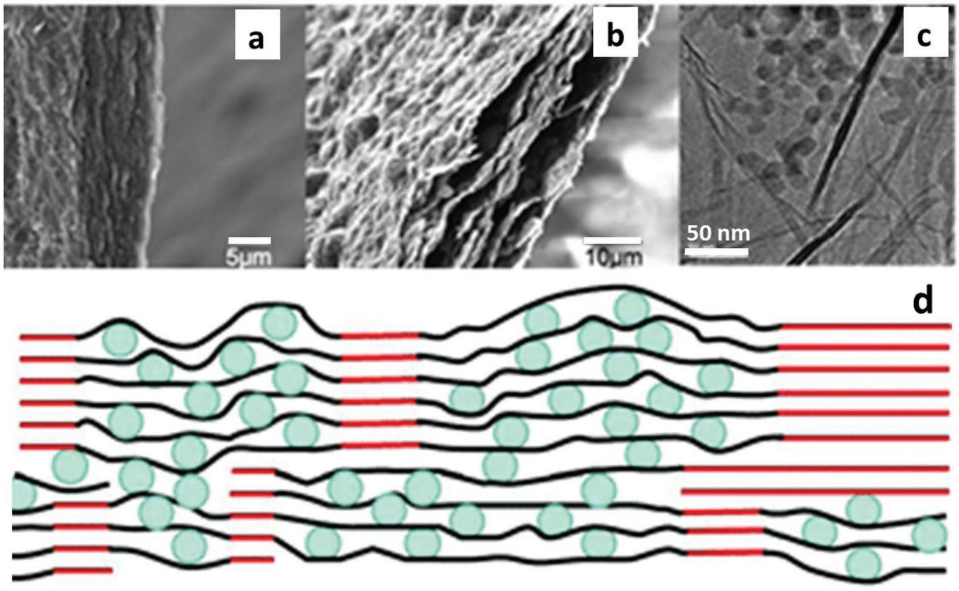

Figure 10. Cross-sectional SEM images of a) SGO paper, and b) SG paper. c) TEM image of SG paper. d) A schematic drawing of SG paper. Reproduced with permission.[84] Copyright 2010, Royal Society of Chemistry.

failing due to Si pulverization, and the carbon coating provide a conductive network for Si. The created void between Si and C allows sufficient space for Si volume change, and helps improve the structure stability. The pores on the carbon shell can function as active Li^+ diffusion pathway. The composite exhibited long cycle life and good rate capability, with 80% capacity retention after 400 cycles, and 62.3% capacity retention when a high current density of 8.4 A g^{-1} was applied.

3.2. Si/Graphene and Si/CNT Composites

Fundamentally speaking, graphene is a monolayer carbon allotrope with 2D morphology. Carbon atoms are chemically bonded in a hexagonal pattern similar to that of a planar honeycomb. Although the existence of 2D monolayer graphene crystal was widely accepted by scientists, it was not until 2004 that the miraculous superstar material made its inception.[80] In just over a decade, graphene has attracted tremendous attention and research interests from a wide spectrum of areas owing to its spectacular electronic, mechanical, and surface properties.[81] By applying different synthetic routes, graphene with different characteristics and properties can be prepared for various applications. In the case of LIBs, graphene has demonstrated good capability in reversibly storing Li,[82] as well as improving the performance of both cathode and anode materials.[83] With an excellent electrical conductivity and superb mechanical properties, graphene has also been able to greatly relieve the symptoms with Si anodes. The research progress of the application of graphene in Si-based LIB anodes will be highlighted in this section.

Research on the combination of Si and graphene began to surge since 2010, six years after the discovery of graphene.[84–86] Lee et al. first reported the application of graphene in a Si NP/graphene paper composite.[84] Graphene adopted in their work was from the reduction of graphene oxide, prepared by the oxidation and exfoliation of graphite, which is a well-established method for the fabrication of graphene at a lab scale.[87] Si NPs were dispersed in water using sonication, and graphene oxide (GO) was later on added to the suspension. The aqueous mixture was further sonicated for uniform dispersion before the mixture was poured into a filter with vacuum suction. A thin paper-like Si-graphene oxide (SGO) composite was obtained. The self-supporting paper was used as electrode directly after the reduction of GO at 700 °C in Ar/H_2 atmosphere. **Figure 10**a is a microscopic cross-sectional view of SGO paper. Figure 10b shows the same composite after reduction of GO. Si NPs and reduced graphene oxide (rGO) sheets can be observed from Figure 10c. Figure 10d is the schematic illustration of the SG composite, where Si NPs are anchored in between layers of graphene sheets. The restacking of graphene sheets leads to the formation of graphite at the sites where Si NPs are not present. The intimate wrapping of Si NPs in graphene sheets enhances conductivity of the SG composite, and the restacking of graphene sheets at some parts can promote the conductivity of the composite at both horizontal and vertical directions. In addition, the paper-like composite achieves better mechanical strength from the partial restacking of graphene sheets. As the pioneering work of Si/graphene composite, the SG sample retained 50% of its original capacity after 300 cycles, much improved from bare Si NPs. The temperature effect of the reduction of GO was also examined, together with the ratio of Si NPs in the SG paper. More Si/G composites have been reported from the combination of Si NPs and graphene, including Si/G particles, free-standing films, and highly porous sponge-like composites, etc.[86,88]

In addition to Si/G composites built with Si NPs and graphene precursors, some auxiliary agents have been integrated with Si/graphene composites to further improve the performance of Si alongside graphene. These additives include

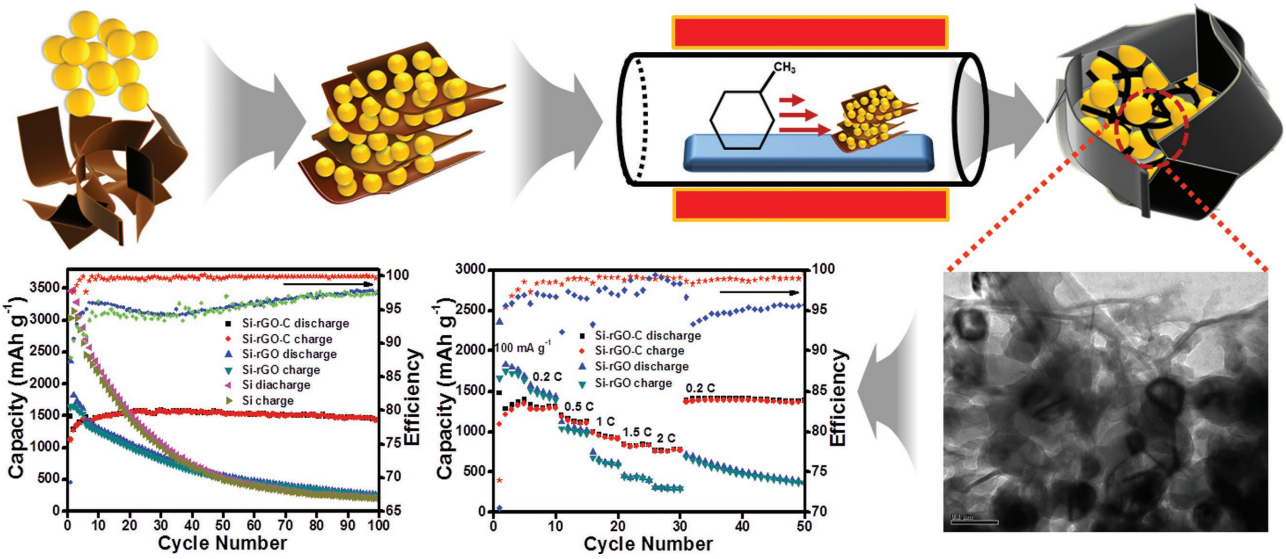

Figure 11. Schematic illustration of the synthetic procedure, TEM image of the Si–rGO–C composite, cycling performance of Si–rGO–C and Si–rGO composites at different rates, and comparative cycling performance of Si–rGO–C, Si–rGO, and bare Si electrodes. Reproduced with permission.[91] Copyright 2016, Elsevier.

alloying and doping agents, polymers, amorphous carbon, graphite, etc.[89,90] Our group designed an in situ carbon network in Si/graphene composite with carbon coating on Si NPs and carbon rods interconnecting Si/graphene flakes.[91] Schematic presentation of the synthesis, a TEM image, and the electrochemical performance are shown in **Figure 11**. Si NPs and GO were first homogeneously dispersed in water and freeze dried. The as-obtained sponge-like Si/GO composite was then placed in a CVD furnace from which GO was reduced in an inert atmosphere at an elevated temperature. Meanwhile, the additional carbon coating and carbon branches were realized by the CVD growth from a carbon precursor, namely, toluene in this case. The material was first examined by several essential physical characterization techniques, studying the morphological and compositional features of the sample. These techniques included thermogravimetric analysis (TGA), Raman spectroscopy, X-ray diffraction (XRD), SEM, TEM, energy dispersive X-ray spectroscopy, and X-ray photoelectron spectroscopy (XPS). It was found by TGA that Si weighed more than 70% in the composite. XRD confirmed the successful reduction of GO to rGO, and the retention of the crystalline phase of Si NPs. SEM and TEM were used to investigate the morphology of the composite. The lower-right image in Figure 11 is a TEM image of the Si–rGO–C composite; Si NPs can be seen well wrapped by rGO, and the created carbon branches interconnect graphene sheets. Compared to the Si–rGO composite without auxiliary carbon, the 3D Si–rGO–C shows much improved cycling stability at different charge and discharge rates, and the CE of the composite reaches above 99%. The composite shows no obvious decay after 100 cycles at a rate of 0.2 C, while electrode from bare Si NPs and Si–rGO composite loses most of their initial capacity over cycling, despite relative higher capacities were reached at the beginning. The CE of the prepared composite is also much higher over the bare Si NPs and Si–rGO composite. EIS confirms that Si–rGO–C possessed a lower initial resistance and displayed minimal increase in impedance over cycling compared to other two electrodes, indicating both better conductivity and more stable structure. The superior performance of the Si–rGO–C composite can be largely attributed to the effect of rGO wrapping and introduction of additional carbon, both of which help form a conductive and protective network for Si NPs.

Apart from the composites and derivatives from the combination of Si NPs and graphene, Si and graphene have been integrated together via other methods, where various morphologies of Si or synthetic methods of graphene are adopted. Si ranging from 0D particles to 1D NWs or nanofibers, 2D nanofilms, and 3D porous structures has been reported,[48,63,92,93] and preparation of the used graphene varies from graphite oxidation and reduction, thermal exfoliation, to CVD growth.[94,95]

Another publication of interest is work by Ji et al.[96] The material was synthesized by simply mixing surface modified Si NPs with graphene oxide followed by drop casting on ultrathin graphite foam (UGF). After thermal reduction of GO, the electrode consisted of a graphite foam with rGO wrapped Si NPs deposited on its surface. The material was able to deliver up to 983 mA h g^{-1}, calculated based on the mass of the whole electrode. Compared to other work based on typically Cu foil current collectors of which the total electrode capacity are much lower (24 mA h g^{-1}) if the mass of the Cu foil is taken into account. The high electrode capacity in this work was the result of the UGF current collector, while the cycle stability was more the effect function of the graphene encapsulation of Si. However, the cycle life of Ji's batteries were relatively poor compared other current Si/graphene composites, displaying a quick decline to only about 50% after a mere 100 cycles. Conceptually simple, the design is to take advantage of the ability of crumpled graphene sheets to expand and contract according to the volumetric change of Si particles, while the high surface area of UGF allows for a uniform and thin layer of Si NPs, which created a 3D electron conductive carbon highway.

Our group used rGO as a support for the growth of Si NWs and obtained a composite with Si NWs anchoring into the corrugated rGO nanosheets.[97] The precursor for the growth was $SiCl_4$, circumventing the toxic SiH_4 widely reported elsewhere, while nickel NPs were used as the catalyst, avoiding the commonly employed expensive gold catalyst for the CVD growth of Si. We utilized a silicide-assisted vapor–solid–solid mechanism, instead of VLS. The reaction occurred at 900 °C, well below the eutectic point of Ni–Si system (993 °C) required for the VLS growth of Si NWs. The stability of the obtained rGO–SiNW electrode greatly improved the cycling stability over bare Si NW electrode. After 30 cycles at various rates of up to 10 A g^{-1}, the cell was cycled at 2 A g^{-1}, and it remained highly stable with minimal capacity decay. This is a typical example of the implementation of 1D Si with graphene as LIB anode materials. Evanoff et al. reported a type of 3D porous micrometer particles made from curved 2D graphene sheets with a thin layer of CVD Si coating.[63] A thin film of Si on the surface of elastic graphene sheets can accommodate the volume change of the electrode during the cycling, and the specific surface area of a 2D film is smaller than that of the Si NPs and NWs, which is good for the stabilization of an SEI layer. The composite exhibits both good cycling stability and CE, with stable capacity retention of above 1000 mA h g^{-1} at 1.4 A g^{-1} and 99% for CE.

CNT is another emerging star in a wide spectrum of applications, including drug delivery,[98] energy conversion and storage,[99] environmental applications,[100] etc. Like graphene, CNTs have also attracted intensive research interest in the combination with Si. CNTs can not only provide very good conductivity to LIB electrodes as a conductive agent, but also provide effective conductive network for Si when integrated with Si as Si/CNT composite. In general, there are three approaches to synthesize Si/CNT composites, namely, physical mixing, chemical bonding, and direct deposition of Si on CNT or CNT on Si. Physical mixing is a simple and effective way to improve good conductivity of Si composite, with the disadvantage of low homogeneity and thus lack of consistency in cycling performance.[101] Chemical bonding can provide a more intimate connectivity between CNTs and Si, however, the C—Si bonds inevitably cause defects in the structure of CNTs. These defects lead to the decrease of conductivity, which is less favorable compared to the surface–surface interaction between CNTs and Si.[102] There has been research focusing on both the deposition of Si on CNTs and CNTs on Si.[101]

Si/CNTs composites for LIB anodes debuted a decade ago,[103,104] since when significant efforts have been reported on the development of various Si/CNTs composites.[105,106] In 2006, amongst one of the earliest reported research on Si/CNTs, Shu et al. exhibited a cage-like CNTs/Si composite, where coiled CNTs were grown on the surface of Si with 1–2 μm in diameter.[104] The in situ growth of CNTs on Si particles displayed much improved wrapping than mechanically milled Si/CNTs composite. Authors also studied size effect of CNTs on the electrochemical performance of Si/CNTs composite. By varying the growth time, CNTs with average length of 400 nm and diameter of 30 nm, and CNTs with average length of 15 μm and diameter of 80 nm were grown on same batch of fine Si particles. The cage-like composite with long CNTs outperformed the one with shorter length in term of cycling stability. While the wrapping of CNTs on the surface of Si can provide an effective conductive network and SEI stabilizing matrix, enhanced wrapping with longer CNTs can further facilitate the electrochemical performance of Si/CNTs composite. A reversible capacity of 940 mA h g^{-1} was achieved after 20 cycles, with 80% capacity retention, which was a significant improvement over bare Si particles and superior over the Si/CNTs with shorter CNTs.

In addition to the physical mixing or chemical bonding of readily made Si and CNTs, the exceptional mechanical and structural properties of CNTs also inspire researchers to develop more unconventional Si/CNTs composites or electrodes. Wang et al. reported a heterostructure composed of nanosized Si dots deposited on vertically aligned CNTs (VACNTs) via CVD.[65] In their work, VACNTs were first grown on a quartz substrate via CVD using xylene and ferrocene as the precursor and catalyst respectively. SiH_4 gas was subsequently purged into the system for Si growth. Both SEM and TEM confirmed that Si nanocluster was firmly attached to the wall of CNTs. The average diameter of the VACNTs was measured to be 40–50 nm. The average size of Si nanocluster was around 40 nm. The Si/CNTs composite was then scratched from the quartz substrate and made into slurry before being cast on copper foil. The composite exhibited a specific capacity of more than 2000 mA h g^{-1} for the initial cycling, and displayed minor capacity decay over first 20 cycles. More interestingly, the capacity loss was decreased to 19.7% in the first cycle, which was a significant improvement over most Si/CNTs composites. The authors approached the explanation of the phenomena via the surface area decrease of the composite. The specific surface area of the pristine VACNTs was around 240 m^2 g^{-1}. Interestingly, the amount of Si deposition was found to be in a linear relation with the reduction of specific area. VACNTs function as the core of the Si/CNTs composite, and provide excellent mechanical and electrical properties and therefore enhanced kinetics for both electrons and Li ions. Meanwhile, the deposition of Si nanocluster helps reduce the specific surface area of the composite, and significantly alleviate the irreversible capacity loss in the first cycle, which is of great interest for practical applications.[107]

Another notable design that preceded the idea of direct growing Si on CNTs was reported by Fan et al.[108] They directly grew CNT arrays on a nickel or stainless steel substrate, which subsequently served as a current collector. Si was grown on the outer wall of CNTs and formed a Si/CNT core–shell structure. CNTs were directly grown on a Ni/SS substrate via a plasma-enhanced CVD method. The Ni/SS with VACNTs was then used as a substrate for Si coating in a RF-magnetron sputtering system. An inverse cone shape Si/CNT structure was expected since the top of CNTs were more exposed to the sputtered Si. **Figure 12**a is an SEM image of VACNTs grown on the substrate. The length of the CNTs varies, while the uniformity of vacancy was well controlled. Figure 12b,c shows the tilted and vertical view of the cone structure of the Si/CNT composite, with a visually apparent larger diameter on the top of Si/CNTs cones. The cone structure could be more beneficial than the uniform coated Si on CNTs in that the volume change of Si on the top of CNTs has less effect on the connection between CNTs and the substrate at the root. In addition, the Si on the top possesses better contact with electrolyte and provides

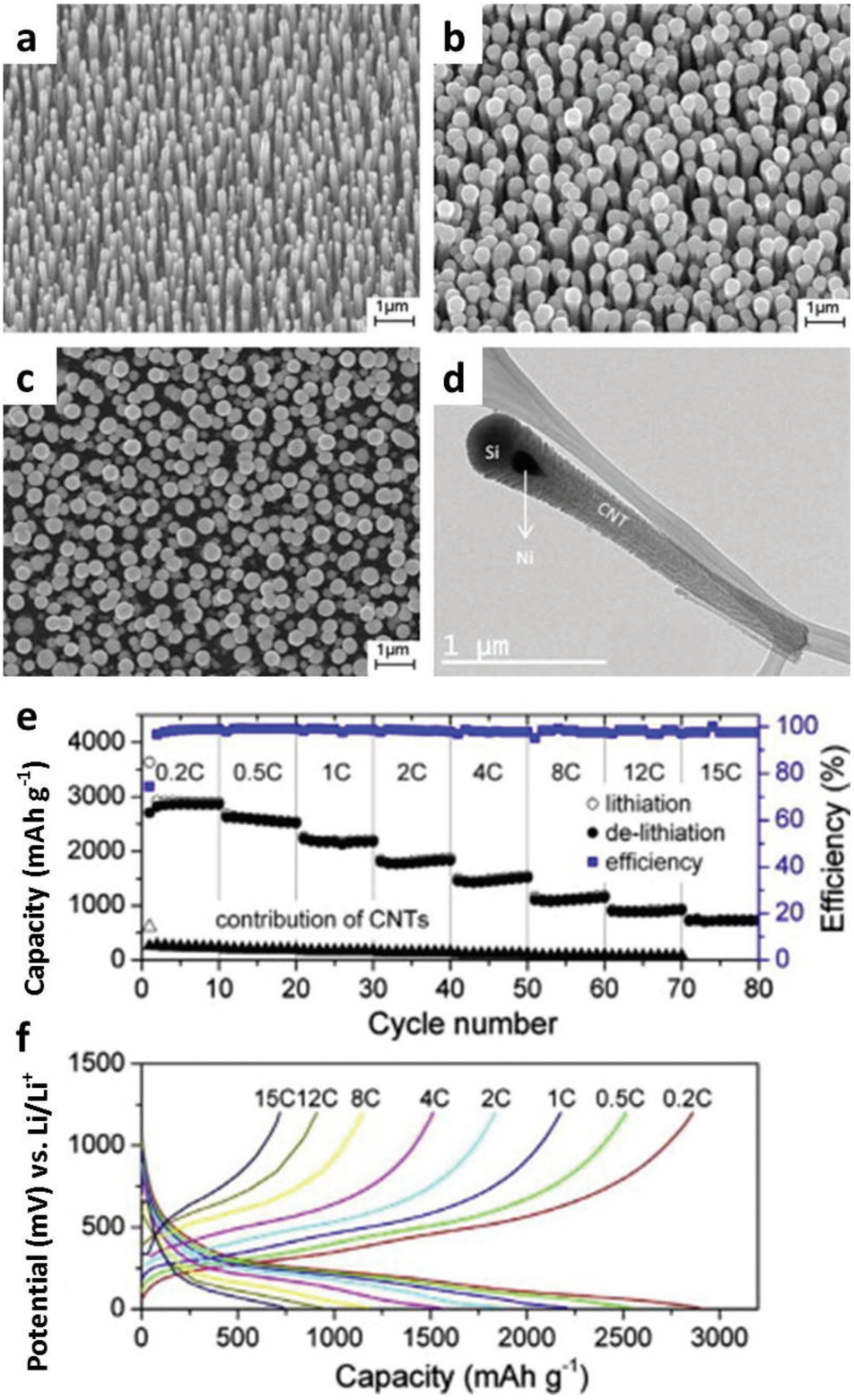

Figure 12. a) Tilted angle SEM image of vertically grown CNT arrays. b,c) Si coated CNT arrays from different angles of view. d) TEM image of a single Si/CNT nanowire, with nickel seed inside. e) Cycle test of Si/CNT composite with charge and discharge rate of up to 15 C. f) Potential/capacity profiles of the cycle tests at various C rates. Reproduced with permission.[108] Copyright 2013, Elsevier.

faster Li-ion kinetics. A single piece of Si/CNT cone was capture by TEM shown in Figure 12d, in which Si, CNT, and Ni catalyst for CNT growth was clearly shown, and Si was seen closely attached to the wall of CNT. As shown in Figure 12e,f, the composite exhibited excellent durability at different rates, and retained more than 1150 and 700 mA h g^{-1} at 8 and 15 C, respectively.[108]

3.3. Si/Conductive Polymer

Conductive polymers such as polyaniline (PANI) and polypyrrole (PPy) have gained popularity among researchers across many different fields. These polymers can yield unique morphologies such as PANI flowers, nanospheres, etc. tuned by the temperature, pH and other reaction parameters. This represents a very tunable design approach for Si/polymer composite. Accordingly, many researchers have implemented them in a Si anode.[109] A relatively unique use of PPy was demonstrated by Du et al. as a protective coating layer on a porous-hollow Si sphere (PHSi).[110] The benefit of this PPy coating can be easily observed in the performance comparison between the uncoated and coated PHSi. The performance of bare PHSi was able to deliver over 3000 mA h g^{-1} on first discharge but with a low retention of 44% over 100 cycles. Without a coating to protect the Si, PHSi succumbs to the symptoms of constant volumetric expansion and retraction of Si material allowing for the continuous formation of fresh SEI layer. The consumption of electrolyte over cycles would increase the diffusion resistance, and compromise the cycle life. In contrast, PPy@PHSi was able to retain 88% of its initial 2500 mA h g^{-1} discharge capacity over 250 cycles. To investigate the reason for the increase in performance, Du proved the robustness of PPy@PHSi through EIS test, SEM, and TEM, indicating a clear lack of change in morphology (cracks) and resistance throughout cycling. The absence of any surface morphological change implies that a stable SEI layer could have been formed on the surface of PPy@PHSi. The reason why the PPy-coated PHSi is superior to bare PHSi is likely due to the protection of PHSi surface. Even if the PHSi's volume expansion is not directed inward, the PPy coating can possibly stretch over the expanding Si surface. This circumvents the need of an inward directed volume expansion presented in hollow Si morphologies.

In another work, Wu et al. utilized a Si/PANI composite, synthesized through the in situ polymerization of aniline with phytic acid as the acid precursor and a crosslinker.[111] The result is a unique porous hydrogel structure with Si NPs imbedded in its matrix both wrapped with PANI and interconnected by interparticle polyaniline bridge. This technique boasted a binderless electrode with good manufacturability. The Si/PANI composite hydrogel could be synthesized in a mere 2 min. Furthermore, due to the high viscosity of the hydrogel it could be effectively used as electrode slurry paste and directly casted onto a current collector with impressive battery performance. At 3 A g^{-1} the composited delivered 1100 mA h g^{-1} with voltage plateau still in the range of 0.3 to 0.01 V indicating fast ion transfer derived from the interconnected polyaniline network. Even at high discharge rates such as 6 A g^{-1} the composite was able to deliver a stable capacity of 550 mA h g^{-1} after 5000 cycles. Their group attributed the improved performance to the ability of the hydrogel polyaniline to accommodate the volumetric expansion of Si in addition to providing a protective flexible thin coating to facilitate the formation of a stable SEI layer. Although the loading was low (0.3 mg cm^{-2}) the concept of a 2 min time interval between reaction and electrode casting was intriguing.

3.4. Si/Metal Alloys and Si/Metal Oxide Composites

In addition to the exhaustive survey on Si/C composites, researchers have also explored merits of Si/metal alloys and Si/metal oxide composites as LIB anodes. Alloy metals can play unique roles in Si alloy anodes, despite their ability to reversibly store Li. Germanium, an element in the same group with Si in the periodic table, exhibits a high theoretical capacity of 1624 mA h g^{-1}, and undergoes less volume change during lithiation/delithiation than Si. In addition, the electrical conductivity of Ge is much higher than that of Si at room temperature. The low abundance and high cost of Ge make it difficult to be applied as a major material for LIB anodes. These factors make it advisable to combine Ge and Si as a LIB anode material. Abel et al. researched Si/Ge thin films with different Ge contents.[112] It was found out that the capacity retention of these film electrodes increases with higher ratio of Ge in the alloy. The enrichment of Ge also positively affects the rate capability of the Si/Ge electrode, making both high capacity and good rate capability achievable. Sn, another Li-active element in the same group with Si, has been found contributive to the structure retention of the alloys with Si, and thus the cycle life of these alloy anodes.[113] Other Li inactive metals have also been reported by researchers and attempted in commercial LIBs.[67,114]

Unlike alloys, Si/metal oxide composites usually render a core–shell structure. Similar to the previous concept with Si/C core–shell composites, a layer of coating layer on Si can serve to prevent direct physical contact of Si with the electrolyte. To add on this concept, Lee et al. has created a composite with surface coating layer consisting of a 20–30 nm thick Li silicate and Li titanate, and obtained an impressive boost in performance.[115] The multifunctional layers were believed to contribute to the increase of electrical and ionic conductivities of the composite, and the stabilization of SEI on Si surface. The composite was able to deliver 1000 mA h g^{-1} even after 1000 cycles at 1 C (67% retention). Additionally, rate performance tests were performed and the composite material was able to discharge ≈800 mA h g^{-1} at an impressive rate of 10 C, whereas the uncoated Si's capacity severely declined at a mere 3 C. The Li titanate and silicate coating plays several roles. The most obvious role is to serve as a protective layer like many other coatings, with a different and interesting mechanism. The Li-ion diffusivity is a few times higher in Li titanate (8.36×10^{-11} cm^2 s^{-1}) compared to SEI layer on pristine Si NPs (1.56×10^{-11} cm^2 s^{-1}), which offered a more efficient pathway for Li diffusion. Li titanate also has the unique ability to become electrically conductive upon discharge. Upon reduction, $Li_4Ti_5O_{12}$ is converted to the spinel $Li_7Ti_5O_{12}$, possessing an electrical conductivity of 10^{-2} S cm^{-1}, a large increase from the insulating state 10^{-13} to 10^{-9} S cm^{-1}. This means that as the cell is being discharged, the composite

Table 1. Electrochemical performance and characteristics of some representative Si anode materials.

Categories of Si		Synthesis method	Cycling stability			
			Specific capacity [mA h g^{-1}]	Cycle number	Current/rate	Ref.
Nanosized Si	Hollow Si	CVD and HF etching of template	1420	700	C/2	[13]
	Porous Si	Mg reduction of silica and acid treatment	1200	600	C/2	[15]
	Si nanowire	CVD on substrate	3500	20	C/5	[22]
	Si nanofiber	Electrospinning and magnetron sputtering	1821	1000	C/5	[28]
	Si nanotube	CVD of Si and template removal	2000	50	C/5	[29]
	Si nanofilm	Vacuum evaporation and deposition	3000	1000	12 C	[34]
Micrometer-sized Si	3D porous Si	Thermal annealing and etching of butyl-capped Si gels and SiO_2	2800	100	1 C	[43]
	Pomegranate-like secondary Si	Si@SiO_2 cluster formation and etching	1160	1000	C/2	[51]
Si/C composites	Simple Si/C composite	Pyrolysis of polymers with Si	1200	30	C/10	[71]
	Yolk–shell Si/C	SiO_2 and carbon coating, before removal of SiO_2	1500	1000	1 C	[72]
	Si/graphene	Freeze-drying	840	300	1.4 A g^{-1}	[85]
	Si/CNT	Growth of CNT on substrate and sputtering of Si	2502	100	C/5	[112]
Other Si composites	Si/conductive polymer	In situ polymerization of on Si	550	5000	6 A g^{-1}	[115]
	Si/metal alloy	Evaporation and deposition of Si and Ge	1600	50	Up to 2 C	[116]
	Si/metal oxides	Solution formation of $Li_4Ti_5O_{12}$ on Si	1000	1000	1 C	[119]

becomes more and more conductive. Furthermore, Lee found a constant interatomic distance from the radial distribution function from extended X-ray absorption fine structure. The group claimed this to be proof that a stable SEI layer has formed on the surface of Si NPs.

Table 1 summaries the electrochemical performances of various Si morphologies, structures, and composites. Synthesis methods of different types of Si anodes are provided along with their capacity and cycling information. To fairly judge the promise of a material, many more factors should be taken into consideration. Therefore, it is desirable that researchers in this field put more emphasis on the practical aspects of new materials developed. These aspects may include cost, electrode and fabrication details, full-cell LIB data, etc.

4. Effectiveness of Electrolyte Selection, Binder Design, and Electrode Engineering Toward Practical Si Electrodes

In addition to the tremendous efforts that have been focused on the development of Si structures and composites, other key factors affecting the performance of Si anodes have been broadly researched. Upon selection and commercialization of the most promising active material (Si) architecture, these will be the only main factors left for optimization to improve Si performance. In addition, to realize the practical application of Si anodes, more factors have to be taken into consideration other than specific capacity and cycle stability, e.g., fabrication simplicity and cost, realistic electrode capacity, electrode thickness control, and overall feasibility in actual batteries. While it is demanding for every investigated electrode or method to address all these issues, there is a trend in recent research to cover these practical aspects via combined approaches. The following section will discuss research efforts that have been made on the non-Si components of the cell, and novel electrode designs and engineering techniques.

4.1. Electrolyte Selection

The function of electrolyte is to provide an efficient Li-ion conduction pathway while simultaneously being electronically insulating. In order to obtain high ion conduction efficiency, the electrolyte must possess a high dielectric constant and a low viscosity at common operating temperatures.[116] Furthermore, since Si is acting as the anode, common electrolytes with solvent combination of ethylene carbonate (EC) and diethyl carbonate (DEC) or dimethyl carbonate (DMC), etc. will inevitably be reduced within the lithiation potential range of Si.[117] The only remaining factor for engineers and scientists to tweak is the successful formation of a one-time, stable SEI protecting Si surface from any further SEI growth. As previously discussed in detail, this presents a major problem for Si due to constant volume change, pulverization, and the resulted generation of new surface area allowing for new SEI formation.[118] The mere contraction and expansion of Si further result in the unfavorable detachment of SEI from active material's surface, which again revealed fresh surface area for additional SEI formation. Electrolyte researchers have sought for means to tackle these issues from electrolyte salts, solvents, and electrolyte additives.

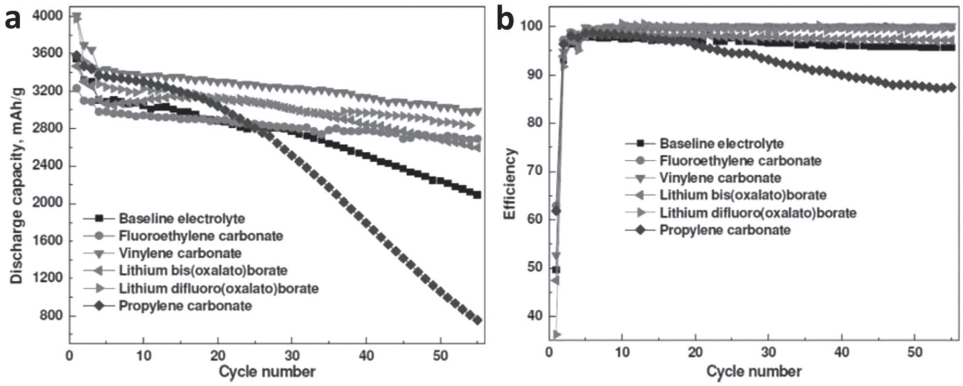

Figure 13. Cycling performance of Si electrodes with various electrolyte additives, in terms of a) efficiency, and b) discharge capacity. Reproduced with permission.[121] Copyright 2012, The Electrochemical Society.

Among these possible solutions, electrolyte salts and solvents are relatively more established due to the intensive research on electrolytes for regular LIBs. Electrolyte additives, which can be specifically elected or tailored to address issues of Si, represent a promising direction in improving performance of Si anodes.

Electrolyte additives, including succinic anhydride,[119] Li bis(oxalate)borate (LiBOB,[120] Li difluro(oxalato)borate (LiDFOB),[121] vinylene carbonate (VC),[122] fluoroethylene carbonate (FEC)[123,124] have been reported to increase both cycle life and CE. An interesting publication by Dalavi et al. has performed direct comparison among most of the above electrolyte additives.[121] Although mechanistic discussion was minimal in this work, it nevertheless provided a good overview of what is expected from each additive under the same experimental conditions. **Figure 13** displays the cycling performance for each electrolyte additive. It is apparent that changing the solvent from EC to propylene carbonate (PC) has quite a detrimental effect on the performance of the cells in terms of cycle life. Additionally, since the cycle life degradation is most likely due to severe SEI formation and reformation, the CE of PC is also very poor. This indicates that at each cycle the PC electrolyte is continuously decomposed with little passivation (protection) effect. This phenomenon is further amplified by pulverization of Si upon cycling, generating even greater surface area for PC to decompose upon. PC-based electrolytes have also been previously reported to be incompetent in maintaining SEI stability, and is known to intercalate into graphite layers, causing exfoliation of graphite layers.[125] When the other additives were compared to each other, Dalavi's work implied that the most effective electrolyte additives are FEC and VC. Both of these additives were able to maintain a high capacity retention and CE.

EC and DEC decompose during cycling, depositing polymeric and oligomeric materials on the surface of Si. $LiPF_6$ decomposes on the surface of the anode active material, be it graphite or Si, LiF is formed in SEI. There have been debates about the role of LiF in SEI, and a comprehensive survey is yet to be accomplished to further understand it.[126] VC decomposes prior to the decomposition of EC and DEC at about 1 V versus Li^+/Li, forming an electrolyte impermeable SEI layer on the surface Si.[127] SEI layer formed by unmodified EC and DEC electrolyte is still slightly electrolyte permeable.[128] It is important to remember the critical properties of an SEI are to be able to transfer Li ions but at the same time remains impenetrable to electrolyte. With the formation of a VC derived initial SEI layer, electrolyte molecules are physically separated from Si and effectively prevented from further decomposition on Si surface.

FEC is one of the most popular electrolyte additives reported in many peer-reviewed articles. Complementing its stable cycle performance, it also has many benefits such as possessing a low melting point and low flammability.[128,129] Since FEC generates VC, it can be expected that it protects the Si in a similar fashion.[124] Xu et al. worked on elucidating the mechanism of which FEC undergoes to benefit as an additive.[130] Similar to previous papers, Xu has compared a FEC-added electrolyte system with an additive-free Si LIB. The result obtained is consistent with previous reports, displaying drastic improvement in capacity retention and CE. Through SEM analysis (**Figure 14**), one can observe the apparent effect of FEC. After cycling for 80 cycles, there appears to be minimal fracturing of the surface of the electrode. Although these fractures are visually observable on the macro scale, it still contributes to the overall increase in SEI formation surfaces. In addition, Si particles in the FEC modified cells appeared to have a significantly more compact SEI layer compared to the bulky SEI layer encompassing the Si particle in the unmodified cells. This would result in a lower mass transfer resistance for the FEC modified cells.

Xu attributed this difference to the fact that FEC decomposes at the voltage of 1.3 V versus Li^+/Li, much higher than that of EC and DEC. From XPS data of the fresh electrode and electrodes discharged to 0.9 V (before the onset of EC and DEC decomposition), there is slight drop in the carbon signal of the SEI layer. In combination with a shift of the C 1s peak from 290 to 290.8 eV, this peak is typically assigned to the carbonate species, but this shift is most likely due the formation of a form of fluorocarbonate, a product likely from the ring opening of FEC.[131] This suggests that FEC is the first to decompose during discharge, providing an opportunity to build a protective layer on the surface of Si before the EC/DEC decomposition occurs.[129] Another benefit of FEC could lie in its ability to form higher fluorinated phosphoric oxides. These new species could interact with and stabilize the intermediate decomposition products of $LiPF_6$, ultimately suppressing any further

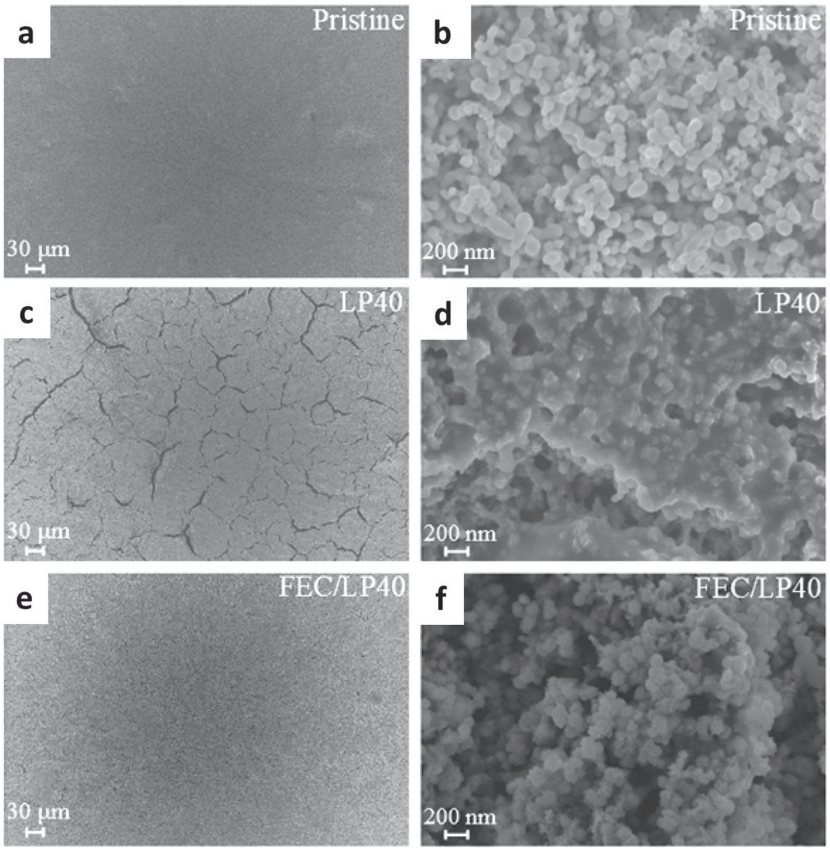

Figure 14. SEM images of: a,b) pristine Si electrodes, and cycled electrodes using commercialized electrolyte LP40 (1 M $LiPF_6$, ethylene carbonate (EC)/diethyl carbonate (DEC)); c,d) with and e,f) without 10% FEC. Reproduced with permission.[130] Copyright 2015, American Chemical Society.

decomposition. To summarize, Xu claimed that not only is the thickness of the SEI an important parameter but also the chemical composition and structural properties of the material. This is conceptually very important, as FEC decomposes on the Si, it effectively creates a Si/polymer composite. Therefore the benefits of FEC are potentially not only in terms of chemistry, but also structural integrity similar to other various Si/C composites. Hence, the mechanical properties, be it the SEI's stiffness or elasticity, could be tuned to provide new direction for future Si LIB electrolyte research.

Some exemplary research on four typical electrolyte additives (FEC, EC, LiBOB, LiDFOB) for Si anodes is outlined in **Table 2**. The plausible working mechanisms and contributions to the electrode performance, and their drawbacks or limitations are also summarized based on the corresponding research.

4.2. Binder Effect

The role of binder in an electrode is to act as a glue to adhere all parts of the electrode slurry together and to the current collector. The binder should also be able to alleviate the stress induced during the electrode drying process, maintaining the mechanical integrity of the electrode. Moreover, the binder should have minimal swelling in the electrolyte, be flexible, conduct Li ions (for LIB), and remain stable in the voltage ranges experienced during cycling. Other more "luxurious" properties of a binder are electrical conductivity, and solubility in nontoxic solvents.[139] In this section, we will discuss what properties of binder are especially influential to the performance of a Si anode; the battery binder should be able to protect the Si from continuous SEI formation in addition to mitigating the volume expansion of Si.

One of the most common binders used for LIB is PVDF and has been a benchmark for comparison, and a topic for scrutiny for many publications in the field of battery binder.[140,141] PVDF has been known to swell significantly in organic solvents, gaining upward of 130% in electrolyte uptake. Chen et al. have showed the corresponding consequence through the swelling ratio test, where the mass of the binder is weighed

Table 2. Electrolyte additives in EC/ DMC, EC/DEC, or EC/EMC based electrolyte systems.

Electrolyte additives	Concentrations and references	Plausible mechanisms and contributions	Performance implications	Drawbacks/limitations
FEC	3%, 25%, and 50%,[123] 10%,[124,130,132] 5–25%[133]	Rapid formation of SEI upon cycling, smooth, thin, and stable SEI, high content of polycarbonate in the SEI	Reduced irreversible capacity, stable cycling, enhanced endurance at high temperature	Relatively lower initial CE, accumulated LiF might be detrimental to SEI
VC	1%,[134] 2%,[135] 3% and 6%,[133] 10%[136]	Smooth and stable SEI, improved polymeric nature, and lower content of LiF in SEI	Improved capacity retention and CE	CO_2 generation, observed increase in cell resistance
LiBOB	5%,[121] 0.13–0.5 M[137]	Reduced consumption of Li and active Si, prevention of decomposition of other electrolyte components	Improved thermal stability, modest improvement in cycling performance	Thicker SEI, relatively less performance improvement compared to FEC and VC
LiDFOB	1%[121,138]	Reduced electrolyte viscosity, stable SEI, higher solubility than LiBOB in carbonates	Good for high and subzero temperatures, forming better SEI than LIBOB, beneficial to both cathodes and anodes	Modest electrochemical performance improvement, high cost

before and after absorption of electrolyte. The percent mass increased is defined as the "swellability." A sufficiently swellable binder loses some of its adhesion ability, which could allow for movement of Si particle upon pulverization and ultimately facilitate detachment of Si material from the conductive matrix.

Another disadvantage of PVDF is the lack of polar functional groups. Its symmetrical fluorine-bonded carbon backbone balances any dipole and can only offer weak van der Waals interaction. That implies that the PVDF cannot intimately wrap around the Si particles. This is particularly disadvantageous as other binders such as carboxymethyl cellulose (CMC), styrene butadiene rubber (SBR) with CMC, Nafion, poly acrylic acid (PAA) and carboxymethyl chitosan all have some form of strong dipole or charge that has been claimed to interact with hydroxyl groups on the Si surface.[142–145] Song et al. reported a PAA–PVA crosslinked binder material for Si, which is rich in hydroxyl and carboxylic acid functional groups.[142] The hydrogen or covalent bonding between the polar groups of the binder and the hydroxyl groups of silica on the surface of partially oxidized Si (**Figure 15**) has been held responsible for better adhesion. Upon repeated lithiation and delithiation, Si and carbon black conductive agent remained trapped inside the interpenetrated gel. The binder effectively enhanced the cycling stability of Si NPs. With an initial capacity of around 2660 mA h g^{-1}, the electrode retained 1830 mA h g^{-1} (68%) after 300 cycles at 1 C. In addition, the electrode delivered a high areal capacity of 4.3 mA h cm^{-2}, comparable to commercial graphite anodes. It is also interesting to note that the active material was commercial Si NPs. Si was directly applied in the electrode fabrication without any further modification or engineering on Si, suggesting that the performance enhancement was achieved

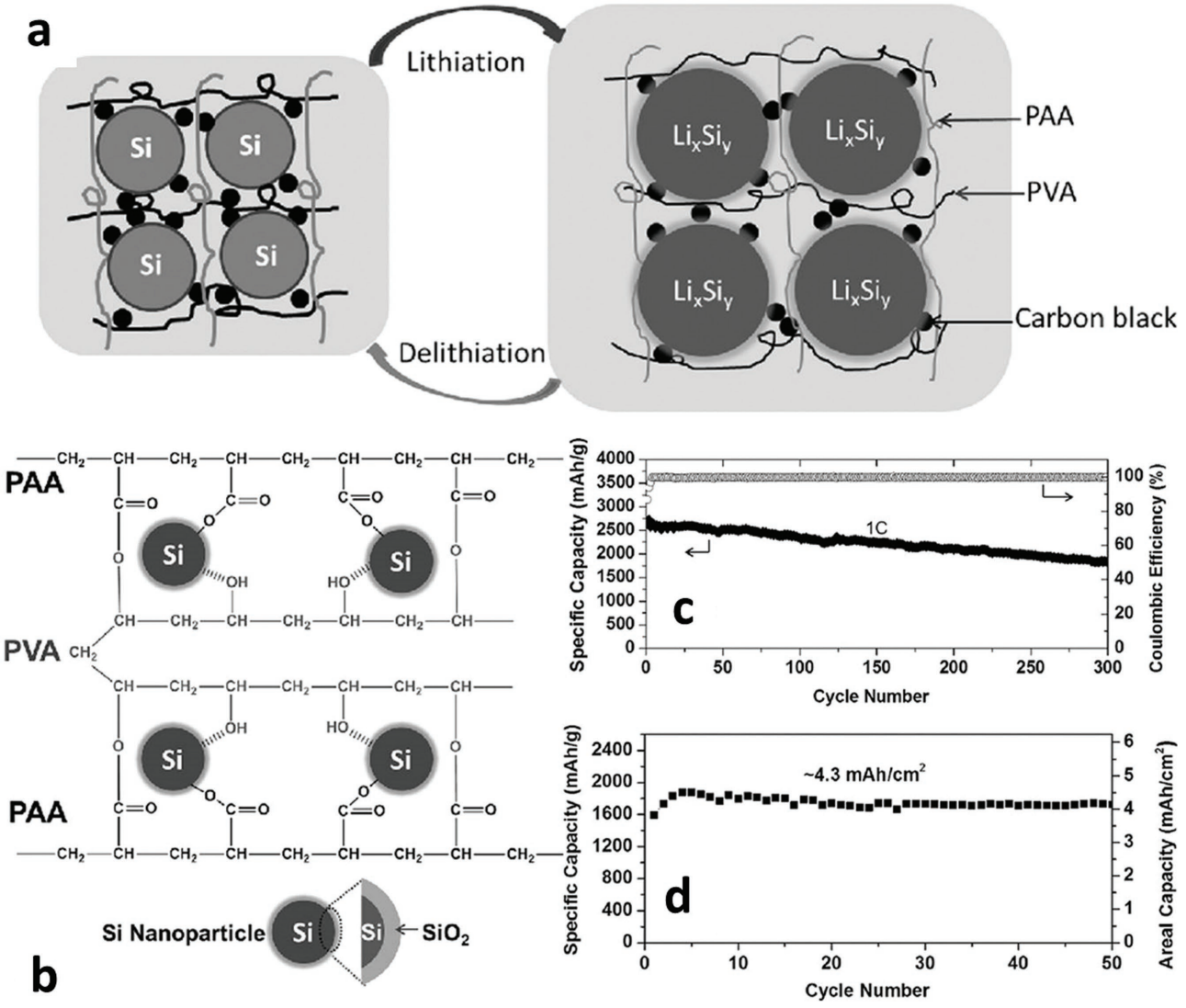

Figure 15. a) Schematic illustration of the proposed working mechanism of the interpenetrated gel binder in a Si anode. b) Chemical structure and plausible chemical bonding between functional groups in binders and partially oxidized Si surface. c) The cycling stability and coulombic efficiency of the Si anode with PAA/PVA binder at a current density of 4 A g^{-1} (1 C), and d) areal capacity of the Si anode with a high Si mass loading of 2.4 mg cm^{-2}. Reproduced with permission.[142] Copyright 2014, Wiley-VCH.

Table 3. Cycle retention of Si anodes using various binders (Si sources, Si loading, and current densities are provided when available).

Binder type	Cycle retention	%Loss/cycle	Anode active material	Si loading [mg cm^{-2}]	Current density [mA g^{-1}]	Reference
Crosslinked chitosan	71% @ 100 cycles	0.29%	Si nanoparticle (Sigma < 100 nm)	N/A	500	[146]
PVDF	0% @ 100 cycles	1%	Si particles (MTI)	0.3	4200	[141]
	5% @ 50 cycles	1.9%	Si nanoparticle (Alfa Aesar < 100 nm)	1.5	400	[142]
Na–CMC	35% @ 100 cycles	0.65%	Si nanoparticle (Alfa Aesar < 100 nm)	1.5	400	[142]
	49.7% @ 200 cycles	0.25%	Si nanoparticle (KCC Korea 60 nm)	0.3	3500	[144]
	82% @ 20 cycles	0.9%	Si nanoparticles	0.6	716	[148]
	42% @ 100 cycles	0.58%	Si nanoparticle (Aldrich < 100 nm)	N/A	300	[141]
SBR–CMC	85% @ 50 cycles	0.3%	Si micrometer particle (99.9% Sigma, ball milled to average 3 µm)	3	300	[151]
β-Cyclodextrin	68% @ 200 cycles	0.16%	Si particles (MTI)	0.6	4200	[141]
PAA–CMC	78% @ 100 cycles	0.22%	Si nanoparticle (Aldrich < 100 nm)	N/A	300	[143]
	88% @ 20 cycles	0.55%	Si nanoparticles	0.6	716	[148]
PVA–PAA	68.6% @ 300 cycles	0.107%	Si nanoparticle (Alfa Aesar < 100 nm)	1.5	4000	[142]
PAA	36% @ 100 cycles	0.63%	Si nanoparticle (Aldrich < 100 nm)	N/A	300	[143]
Native xanthan gum	72.2% @ 200 cycles	0.139%	Si nanoparticle (KCC Korea 60 nm)	0.3	3500	[144]
Alginate	51% @ 200 cycles	0.245%	Si nanoparticle (KCC Korea 60 nm)	0.3	3500	[144]
	27.1% @ 150 cycles	0.486%	Si particles (MTI)	0.3	4200	[141]
PEDOT:PSS	78% @ 100 cycles	0.22%	Si nanoparticles (US Research Nanomaterials 50–70 nm)	1	1000	[152]
PFFOMB	67% @ 650 cycle	0.05%	Si nanoparticle (Aldrich < 100 nm)	N/A	420	[153]

solely through the selection of binder. The electrode fabrication process resembled much of the commercial process. Considering the stable cycle performance, and the high areal capacity, this research has developed a low-cost and scalable approach to fabricate Si anodes, with competitive electrochemical performance compared to commercial graphite anodes.

The benefits of enhanced binders have been further theorized to form a protective layer on the surface of Si, very similar in concept to that of carbon and other polymer coatings (PANI, PPy).[146] Due to hydrogen bonding, certain binders can form a protective layer with Si and even contain pulverized Si particles.[147] In a more recent research published by Cao et al., crosslinked PAA–CMC was utilized as a binder for Si anode.[148] The binder was found to be helpful in the formation of a protective SEI on Si via the reduction of PAA during the first cycle. In addition, the Lewis basic $-CO_2Na$ group, which is rich in the binder, was proposed to nullify generated HF via the following mechanism

$$-\mathrm{COONa} + \mathrm{HF} \rightarrow -\mathrm{COOH} + \mathrm{NaF} \quad (2)$$

This suggests that binder materials can contribute to the improvement of Si battery performance via the stabilization of SEI, in a similar manner to some work on electrolytes. Although hydrogen bonding is important, forcefully increasing polarity of a polymer while compromising other properties such as flexibility is not desirable, indicating an optimization problem. Similarly, a binder with zero swellability is also not desirable and results in drastically decreased Li-ion conduction through electrolyte.[149,150]

Simply having surface interaction is regarded as insufficient in ensuring conservation of electrode architecture. Researchers have claimed that it is possible for binders with long non-branched chains to slide during the volume expansion of Si. Once it slides, it can result in migration of Si toward one another rather than stretching out of the polymer. Researchers have looked to use crosslinked polymers to create a binder super structure preventing interpolymer chain sliding[142–144] and have found impressive improvement in performance as shown in **Table 3**.

However, mitigation of Si structure deterioration alone cannot assure the good cycling stability of Si electrodes. Major challenges for 0D Si nanostructures stem from the loss of electrical contact. In traditional slurry preparation process, Si active material is mixed with a conductive additive and a binder, and the repetitive volume changes of Si over cycling can lead to the disconnection of Si from the conductive network. Binders that possess strong interaction with Si's hydroxyl groups can partially mitigate loss of electrical contact by reducing the migration of Si materials. A more direct approach is use a type of inorganic glue which can fuse Si particles together and bind them to the conductive network or current collector.[154] In Cui's work, a layer of amorphous Si was deposited as inorganic glue over carbon-coated crystalline Si particles on a stainless-steel foil. This method not only demonstrated improvement on cycle life of nano-Si, but also enhanced the stability of micrometer-sized Si in half cell tests. In the electrochemical characterization section, the authors used a constant charge capacity (CCC) technique for their coated electrodes and control electrodes, which limited the capacity and thus the amount of Li that can be inserted in the anode. All electrodes were cycled with an

upper cut-off voltage of 0.9 V, and the lower cut-off voltage was set to 0.01 V. These batteries can be charged and discharged well above the lower cut-off voltage during initial cycles without much capacity decay. The coated Si particles, with sizes of 200 nm, 8 µm, and 15 µm, all showed stable cycling for prolonged cycles compared to bare Si particles.

It is desirable for a binder to be able to deliver electrons to the Si material as it can decrease the chance of Si detaching from the electric circuit. There is no longer a need or firm requirement to ensure a good interface between binder, conductive additive and Si. The Si can more easily maintain electrical contact even if it migrates throughout cycling. Furthermore, because the binder serves the dual purpose of conductive network and binder, conductive additives are no longer needed, raising the overall energy density of the slurry mixture. Wu et al. have synthesized a polymer binder derived from a combination of the following monomers, fluorene with octyl side chains, fluorine with triethylene oxide monomethyl ether side chains, methyl benzoate ester, and fluorenone.[150] Rationally, each component of the polymer was assigned a type of functionality and hence can be used to tune the final properties of the polymer. Other researchers demonstrated improvement in performance after using copolymer of PPy and PAA,[155] crosslinked PAA with PANI polymerized within its structure[156] and methacrylate methacrylic acid-PPy copolymer as binders.[155,157]

Liu and co-workers reported a bifunctional polymer material with tailored electronic structure, poly (9,9-dioctylfluorene-*co*-fluorenoneco-methylbenzoic acid) (PFFOMB), which was found to bear good electrical conductivity and robust mechanical binding with Si.[153] This material can function as both a binder and a conductive agent, and the traditional carbon conductive additives can be eliminated. As shown in **Figure 16**, unlike traditional electrodes made with Si NPs, which suffer from broken electric contacts over cycling, the reported Si/PFFOMB composite can maintain good electrical conductivity, avoiding break-up of Si NPs from the conductive network. This research also confirmed that the PFFOMB polymer has a significantly lower energy level of the lowest unoccupied molecular orbital (LUMO) compared to other binders via synchrotron-based soft X-ray absorption spectroscopy. It was found that the high electrical conductivity of polymers for anodes in reducing environment can only be maintained in polymers that can be cathodically (n-type) doped, i.e., lower LUMO.[158] The highlighted carbonyl and methylbenzoic ester function groups in PFFOMB in Figure 16c are largely responsible for tailoring the conduction band and enhancing the mechanical binding with Si, respectively. The as-prepared Si/PFFOMB anode showed superior stability over other Si composites, including Si/AB/PVDF, Si/PAN, etc. The composite also presented excellent capacity retention after long cycles, with a high efficiency. After 650 cycles at C/25, the specific capacity of Si in Si/PFFOMB electrode still presented 2100 mA h g^{-1}. The CE for Si/PFFOMB electrode mostly remained above 99% over the cycling.

Another type of novel binder materials are self-healing polymer (SHP) binder materials. A notable example is the self-healing chemistry research reported by Wang et al.[147] In their work, micrometer Si particles were used as the active material. Over charge and discharge, micrometer Si inevitably pulverized due to volume change, while the micrometer Si in Si/SHP composite was retained in the SHP coating layer. The conductivity of SHP was realized by blending conductive carbon black NPs into SHP. Abundant hydrogen bonding is the main reason for the self-healing behavior of SHP. Additionally, this polymer's amorphous structure, as well as low glass transition temperature (T_g), could both facilitate the rearrangement diffusion to fractures sites and the subsequent remixing of polymer chains. The conductivity of as-prepared SHP coating on an inflatable balloon was measured to be around 0.25 S cm^{-1} with the addition of carbon black NPs. The value decreased by 10 times once the balloon was inflated, but it was able to restore to its original

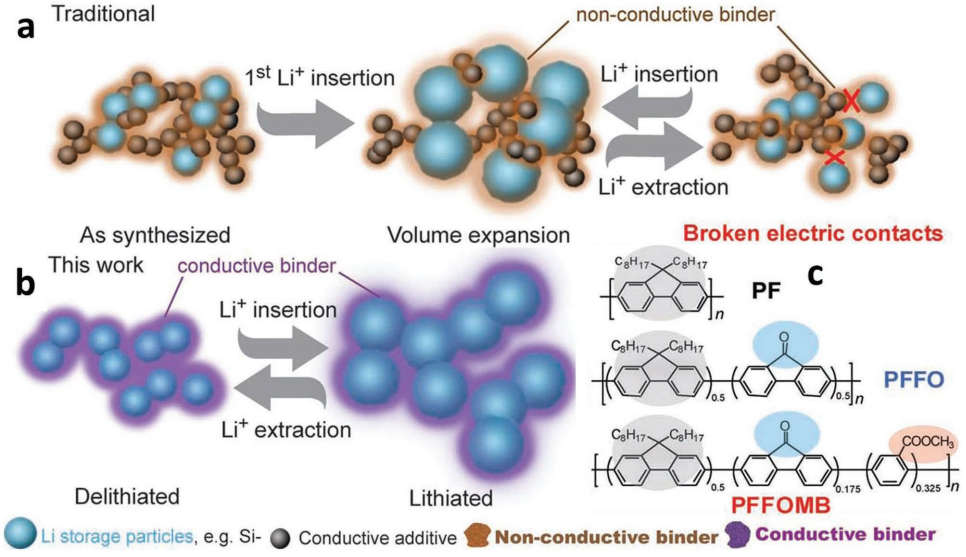

Figure 16. Schematics of a) Si electrode fabricated with traditional binder, before and after lithiation. b) Conductive binder coated Si before and after lithiation, maintains a much better conductive framework than the traditional electrode above. c) Molecular formula of PF-type conductive polymers, and PFFOMB with tailored conduction band and mechanical binding property. Reproduced with permission.[153] Copyright 2011, Wiley-VCH.

value upon full deflation. Si electrode using SHP binder showed much longer cycle life compared to those with traditional alginate, CMC, or PVDF binders. The stability of Si/SHP electrode also revealed good stability at various rates from 0.2 to 2 A g^{-1}. At 2 A g^{-1}, the electrode still maintained a capacity of around 1400 mA h g^{-1}.

4.3. Unconventional Electrode Engineering

Unlike traditional carbon-based anodes and Li metal oxide cathodes, Si faces unprecedented challenges arising from its volume changes, unstable SEI, and some other associated problems. Most efforts on Si have been focused on the design and fabrication of Si materials so far, while the work on electrode design and processing provides another unique route for the improvement of Si electrodes. The efforts on electrolytes and binders have been proven to be effective and practical in improving performance of Si electrodes, and it is encouraging for other research focusing on aspects other than Si structures and composites. To achieve the overall satisfactory performance of Si as practical anodes in LIBs, it is interesting and pragmatic to design and engineer Si electrodes at the electrode scale.

Si NWs were reported to be synthesized directly on a stainless-steel substrate by Cui et al.[159] In their work, traditional binder material and conductive additive were eliminated. Good mechanical and electrical properties of the crystalline-core and amorphous-shell Si NWs enabled long cycle life and fast charge and discharge. The electrode demonstrated high capacity retention after 100 cycles, and excellent rate performance at a high charge and discharge rate of 1.6 C (6.8 A g^{-1}). Their work inspired more researchers to use the similar concepts, extending interests on self-standing electrode materials, bendable and flexible electrodes, and other unconventional electrode designs.[32,93,156] Liu et al. reported a flexible Si electrode with Si NWs spray-coated on a carbon-cloth (CC) substrate. The Si NWs-CC electrode delivered specific capacity of as high as 3000 mA h g^{-1}, and excellent cycling stability with capacity retention of 92% after 200 cycles. It is important to note that the loading density of the active Si NWs on the electrode can reach as high as 3.5 mg cm^{-2} as per calculated, which makes it comparable to commercial graphite electrode with more than 30 mg cm^{-2}, making it potentially applicable in flexible batteries for wearable devices.[160]

Our group has reported a flash-heat-treatment method (FHT), in which the Si-containing slurry was coated to copper foil prior to heat treatment and the subsequent battery fabrication process.[161] In this method, the Si-containing electrode material was in situ synthesized on copper foil substrate, with the elimination of traditional electrode fabrication process. Si NPs and PVDF with a ratio of 6:4 were uniformly dispersed in NMP, without any conductive additive. The Si-PVDF slurry was coated on a regular copper foil and then subjected to the flash-heat-treatment. Specifically, Si electrodes produced via FHT bear several key advantages. First, the synthesis is particularly simple and economical with potential for mass production. Second, the FHT process creates a C/SiO_2 outer shell that can restrict volume expansion of Si and help stabilize SEI layer. Third, a dense and interconnecting network was generated from the carbonization of PVDF, which improved the electrode integrity and boosted the electrical conductivity. Interestingly, a thin layer of graphene was found after FHT treatment with the presence of copper foil, which served as a catalyst for the conversion of carbonized PVDF to graphene. All these factors synergistically contributed to the improved cycling stability and rate performance (1150 mA h g^{-1} after 500 cycles and at a discharge rate of 1.2 A g^{-1}).

Our group has furthered this methodology with the discovery of synergistic effect in the Si–sulfur–graphene system.[162] Sulfur-doped graphene (SG) was first prepared. Similar to the aforementioned FHT method, slurry with 60% Si NPs was prepared in DMF with additives including SG, PAN, and GO. After coating and drying of the slurry on a copper foil, the coated foil was punched into the size of coin cell electrodes. The as-prepared electrodes were placed in a tube furnace and heated at 450 °C in argon atmosphere for the cyclization and partial carbonization of PAN, forming an interconnecting and robust structure containing Si NPs and SG sheets. In this electrode, cyclized PAN and SG synergistically interact with Si and form a unique 3D structure, which provide good elasticity and enough void space to accommodate the repetitive volume change of Si. Stable cycling of more than 2000 cycles at the rate of 1 A g^{-1} was reported, superior than most of the reported work with Si anode, and very competitive among the current commercial anode materials. Further efforts were made to explore the mechanism behind the observed high performance. **Figure 17**a–d display the HAADF-STEM image and the corresponding EELS element mapping for carbon, Si, and sulfur of the selected area. It can be seen that Si is delocalized along the carbon skeleton with high content of S and carbon. Figure 17e schematically depicts how Si is spread onto the SG-cyclized PAN skeleton, avoiding agglomeration of Si during lithiation and delithiation. The binding energy between Si and SG is found to be higher than that of Si on regular graphene from DFT calculations, indicating stronger attachment of Si to SG.

5. Silicon Full-Cell Designs

For early-stage research purposes, Si anodes were commonly tested as a cathode versus Li metal or in what is known as a Si half-cell. With the continuous advancement in Si anode research, there is a trend in academia of pairing the as-prepared Si anodes with commercial cathodes to evaluate the full cell performance. As Si is regarded as an replacement to graphite anodes, the corresponding cathode of choice are $LiCoO_2$,[94,163] $LiFePO_4$,[164] $LiMn_2O_4$,[165] Li-rich cathodes (e.g., $Li_{1.2}Mn_{0.534}Ni_{0.133}Co_{0.133}O_2$),[90] etc.[166] Fabrication of a full-cell Si battery presents a more practical evaluation of the cells and brought research one step closer to practical application. With a full cell, estimates of specific energy, specific power, and overall energy densities can be more accurately evaluated and compared to commercial LIBs with carbon-based anodes. Early work by Cui et al. has demonstrated a Si NW anode of 1 mg cm^{-2} loading paired with a 10 mg cm^{-2} of $LiCoO_2$ was able to deliver 80% capacity retention, similar to the cell with Li metal as anode.[163]

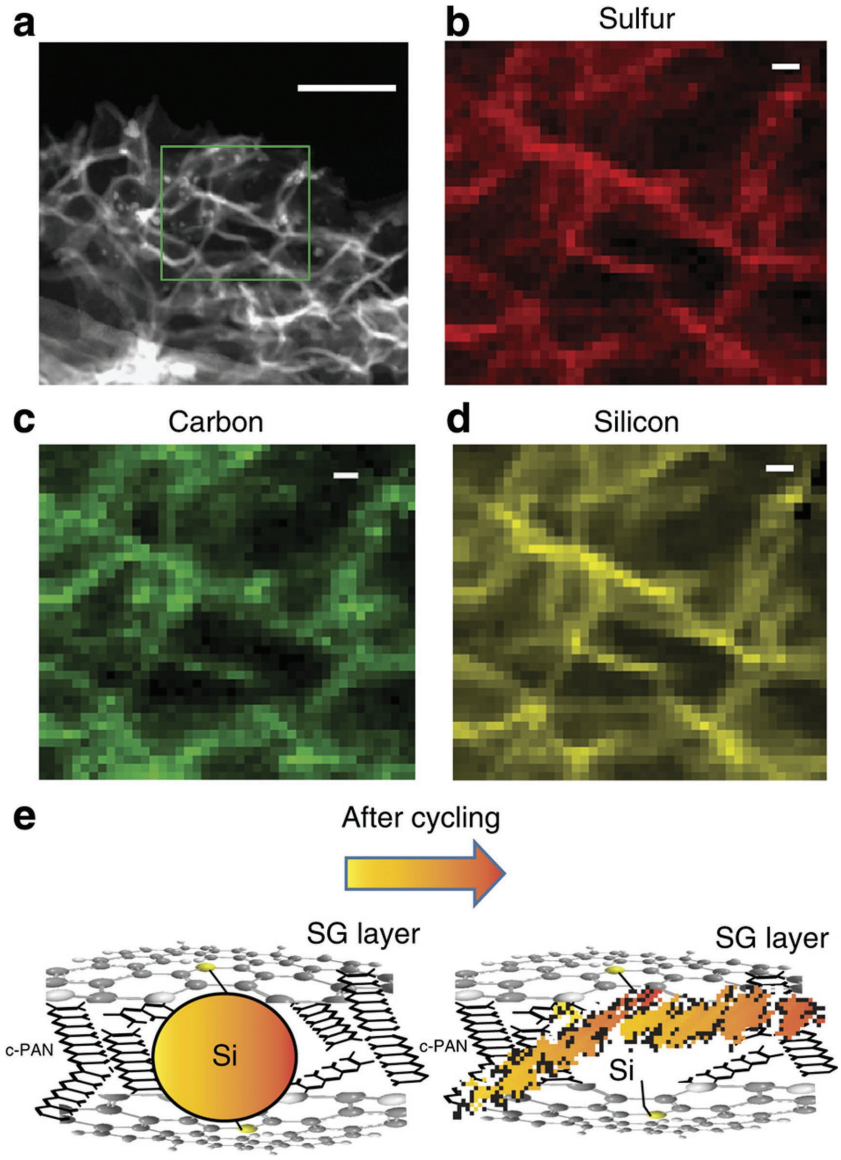

Figure 17. Physical characterization and schematic illustration of the SG–Si electrode after 2250 cycles: a) HAADF-STEM image of the cycled electrode. b–d) Element mapping of sulfur, carbon, and Si of the SG–Si composite, the scale bar represents 100 nm in (a), and 10 nm in (b–d). e) A schematic explanation of the material before and after cycling, illustrating the delocalization of Si onto the surface of SG after Si amorphization and bonding with S. Reproduced with permission.[162] Copyright 2015, Nature Publishing Group.

Furthermore, a commercially comparable areal capacity of 4 mA h cm^{-2} was achieved with the full cell using Si NW anode. Moving on to a recent publication, Son et al. fabricated a full cell in a 18650 type (**Figure 18**) battery with a slightly lower specific areal capacity of 3.8 mA h cm^{-2}, but estimated a volumetric energy density of 972 Wh L^{-1} even after accounting for the thickness of the separator, electrodes, and current collector to be about 105 µm.[94] Compared to the commercial batteries, this Si LIB has an 80% increase in volumetric energy density and has a cycle retention of 72% after 200 cycles. The electrolyte typically used for a Si anode half-cell (1.1 M $LiPF_6$ in EC, DME with FEC additive) was used in Si anode and Li metal oxide full cells.

Interestingly, recent analysis by Pope et al. has forecasted lithium–sulfur battery's gravimetric and volumetric energy density for a given areal loading of sulfur.[167] Although theoretical, this work comprehensively took into account the components in a battery (electrolyte, separator, current collectors, binder, and conductive additives) and should serve as a good indicator of the relationship between areal silicon loading and practical energy densities. Revisiting and applying a similar energy density forecasting model developed by Pope, we have developed a similar but critical relation for silicon anode full-cell batteries, with the widely used $LiCoO_2$ as cathode. Detailed calculations can be found in the Supporting Information.

One important benefit of any energy density forecasting is the identification of the point of diminishing return. Increasing the active material mass loading does not linearly increase the energy density of any given cells. This is due to the other components that scale with increasing active material content such as binder, conductive additive and etc. From **Figure 19**a,b, there appears to be a plateau in both the gravimetric and volumetric energy density for Si based battery at around 15 mg cm^{-2} with noticeable diminishing returns starting at ≈2 mg cm^{-2}. Therefore, from our model it would appear that improvements beyond 15 mg cm^{-2} would be unnecessary for achieving practical Si anodes.

Furthermore, it appears that a Si electrode with an achievable 1000 mA h g^{-1} can surpass the commercial LIB ($LiCoO_2$ cathode and graphite anode) in terms of both gravimetric and volumetric energy density. The theoretical energy density of a $LiCoO_2$ paired Si full cell can be found as the 4200 mA h g^{-1} curve (Figure 19a,b), indicating a maximum gravimetric energy density of 410 Wh kg^{-1} and a volumetric energy density of 1570 Wh L^{-1}. Assuming a discharge capacity of 3000 mA h g^{-1} when normalized against silicon, and a relatively low areal loadings of 2 mg cm^{-2}, such cells are forecasted to possess roughly 1100 Wh L^{-1} and 300 Wh kg^{-1}. While 300 Wh kg^{-1} is a minute increase from commercially available LIBs, the volumetric energy density (1100 Wh L^{-1}) is almost double. Certain applications of batteries require different operating parameters such as volume versus mass based energy density. When paired with a $LiCoO_2$ cathode, a Si full cell can be applied in volume sensitive applications such as portable electronics. Depending on the cathode, a Si full cell can be tuned to different applications.

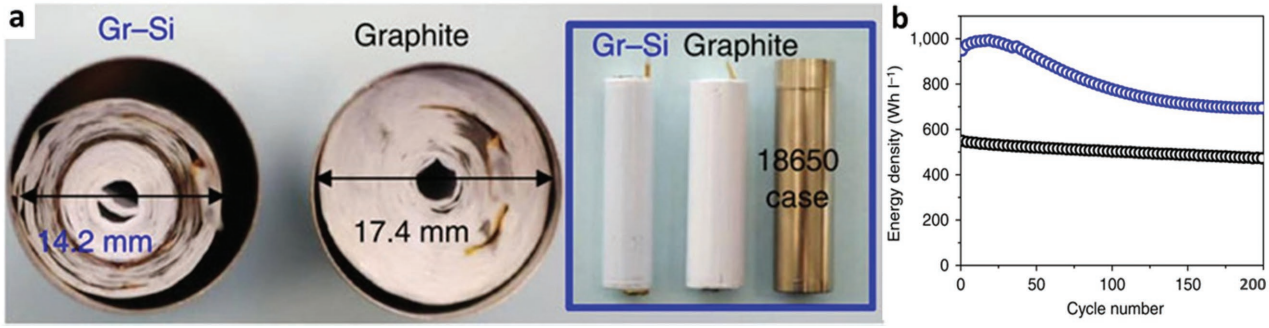

Figure 18. a) Realistic illustration of increase in volumetric energy density from graphite to Gr–Si electrode in an 18 650 cell case. b) Volumetric energy density versus cycle number of Si full cell (blue, upper) and commercial LIB (black, lower). Reproduced with permission.[94] Copyright 2015, Nature Publishing Group.

In addition to the traditional Li metal oxide cathodes, another popular field of research is the sulfur cathode. Research publications in sulfur battery usually dubbed the technology "lithium–sulfur battery" (LiS) implying the use of a Li metal anode. Regarded as the holy grail of battery technology, a Li anode for LiS possesses many advantages but simultaneously is plagued with a plethora of technical challenges. From a safety and cycle life point of view, the anode currently could not be viewed as commercially ready for secondary batteries. In its place, Si has a great potential in being a safer and easier candidate to implement. According to our Figure 19c,d, a SiS cell would be superior to a Si/$LiCoO_2$ batter in terms of gravimetric energy density. However, a SiS cell is in actuality inferior to a Si/$LiCoO_2$ battery when comparing volumetric energy density. This is understandable because of the drastic decrease in active material density (4.9 g cm^{-3} of $LiCoO_2$ to 1.96 g cm^{-3} of sulfur).

Research on a Si–S LIB (SiS) has only recently increased, with less than 20 publications from 2011 to 2016. This is most likely due the difficulty in implementation of both the Si anode and the sulfur cathode. The challenges of a sulfur cathode mainly stems from the electron insulating nature of sulfur and the dissolution of the sulfur into electrolyte during discharge and charge leading to the polysulfide shuttle effect. With research in both areas booming, researchers have finally dedicated some tentative efforts on the SiS battery. As the SiS battery does not contain Li metal, the Li has to be incorporated in the cell through some lithiation procedure, with the possibility in both cathode and anode. Whether the sulfur or the Si electrode is to be prelithiated is still not well established with researchers adopting both methods (Si lithiation[168–171] and sulfur lithiation[172,173]). The method of lithiation also varies significantly between groups with researchers utilizing pressure activated stabilized-lithium-metal-powder (SLMP),[106] half-cell lithiation,[171] use of purchased Li_2S.[172] One important advantage of half-cell lithiation is the activation and stabilization of either the Si or sulfur electrode prior to full cell assembly. This provides the full cell with at least one stable electrode to cycle. Obviously, this method is less practical as it requires an

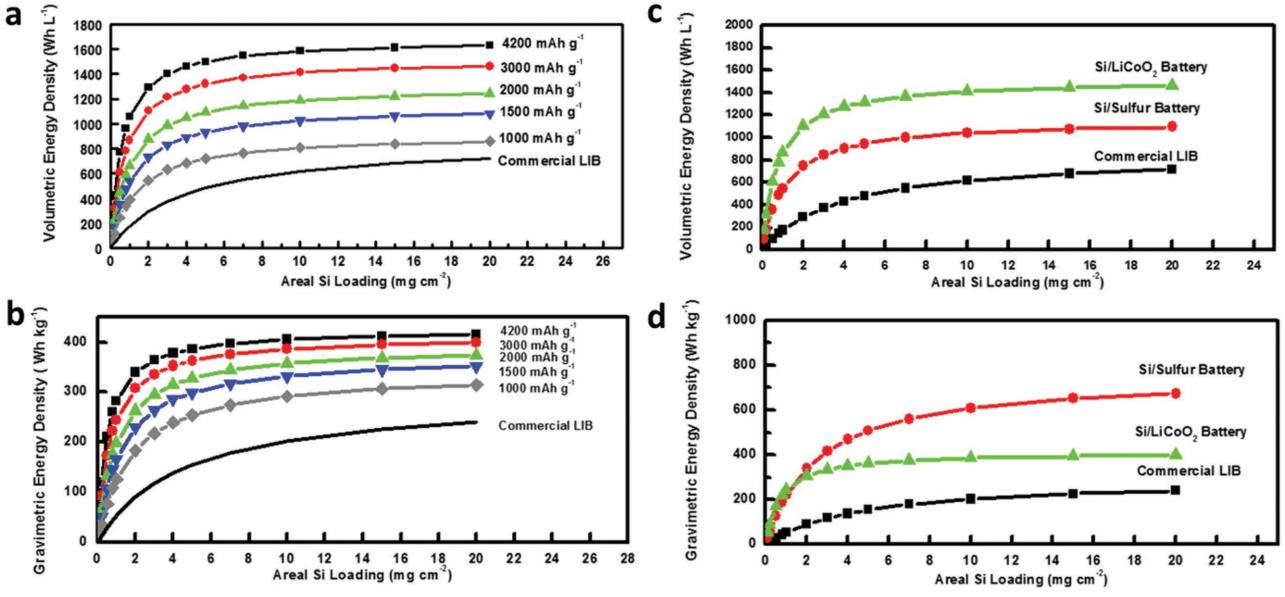

Figure 19. a) Volumetric and b) gravimetric energy density of Si/$LiCoO_2$ full cell at various discharge silicon capacities. c) Volumetric and d) gravimetric energy densities of a Si full cell paired with different cathode materials.

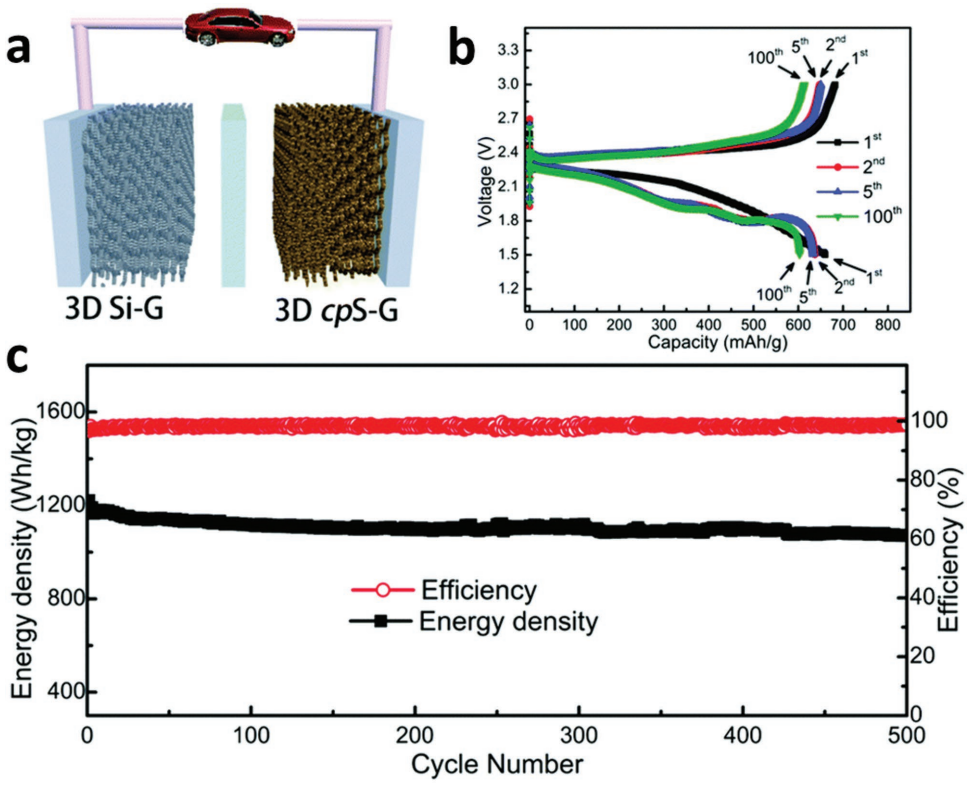

Figure 20. a) Schematic illustration of a newly configured lithiated Si–S battery onto 3D graphene networks. b) Selected voltage profiles of a lithiated Si–S battery from 1st to 100th at 0.27 A g^{-1} based on the total mass of the cathode and anode. c) Long cycle performance of the full lithiated Si–S battery built on 3D graphene. Reproduced with permission.[175] Copyright 2016, Royal Society of Chemistry.

extra step in manufacturing whereas usage of SLMP includes a simple modification to the slurry composition but with more sophisticated raw material.

In terms of electrolyte selection, there has been minimal to no research on the effect of different electrolytes on a SiS system with most SiS publications utilizing LiS electrolyte. This electrolyte usually contains lithium bis(trifluoromethanesulfonyl) imide (LiTFSI) and Li nitrate ($LiNO_3$) in 1,3 dioxolane and dimethoxymethane.[169,172] Another choice of electrolyte is Li trifluoromethane sulfonate ($LiCF_3SO_3$) salt in tetraethyleneglycole dimethylether (TEGME) solvent,[168] also an electrolyte used in LiS field of research. Selection of such electrolytes is mainly to avoid the nucleophilic attack of carbonate-based electrolytes by polysulfide species.[174]

A recent publication from Li et al. elaborated a full lithiated Si–S cell, in which a honeycomb-like S copolymer on 3D graphene was used as the cathode and a 3D lithiated Si-G network was employed as the anode.[175] Both the cathode and anode utilized the 3D graphene as the backbone for the loading of Si and S (**Figure 20**a). The 3D electrode structure was claimed to provide the necessary high electronic conductivity and buffer space for both the Si and S volume change. The S copolymer on the 3D graphene network possesses large amounts of covalent bonds, inhibiting the dissolution of polysulfides. Selected voltage profiles of the fabricated Si–S cell were displayed in Figure 20b at a current density of 0.27 A g^{-1}. Despite being lower in operating voltages than that of commercial LIBs, the reported Si-S cell exhibited an overall energy density of more than 1100 Wh kg^{-1}, which is much higher than that of the commercial cells with energy densities less than 300 Wh kg^{-1}. More than 86% of its initial capacity was retained after 500 cycles, corresponding to a decay rate of only 0.028% per cycle.

6. Summary and Outlook

Over the past two and a half decades, LIBs have rapidly emerged as an indispensable part of our society, rooted in the application of a wide range of portable electronic devices, as well as other large scale devices or projects. However, as the current LIBs are approaching their theoretical capacity limits, there is little room to further increase their energy density by improving battery design based on the traditional materials science and methodology. The high-energy demand from applications including EV has intensively fueled the quest and research for new LIB technologies that were previously thought to be impractical. Si exhibits a theoretical Li storage capacity as high as 4200 mA h g^{-1}, much higher than that of the currently dominating carbon-based anodes. Along with its high abundance and good environment compatibility, Si has been deemed as a potential replacement of carbon-based anodes and garnered tremendous research attention. This review has illustrated the advantages of Si anodes, together with the operating mechanisms and underlying challenges that remain to

be solved for the successful commercial implementation of Si anodes. During a typical lithiation process of Si anode, pristine Si alloys with Li, and forms different types of Li_xSi_y, depending on the degree of lithiation. The theoretical stoichiometric limit of the lithiation of Si is the formation of $Li_{22}Si_5$, corresponding to the aforementioned high capacity. It is also important to note that both lithiation and delithiation of Si versus Li^+/Li are below 0.5 V, lower than most other alloy-type or metal oxide anodes. This can contribute to a high operating voltage of a full-cell LIB, and thus a high energy density. During the lithiation and delithiation process in a bulk Si anode, there exists both substantial Li concentration gradient and stress gradient. Further considering the semiconducting nature of Si, the actual capacity is expected to be lower, and the electrode structure is prone to fracture due to 300% volume increase upon full lithiation. To make matters worse, an unstable SEI repetitively grows, isolating the active material, and drains electrolyte. The volume effect and unstable SEI finally lead to the pulverization of electrode, low CE, and short cycle life of Si-based LIBs.

A comprehensive discussion of various research directions targeting these issues has been presented. To begin with, it is crucial to engineer Si to be below a certain dimension to avoid structure failure due to volume change. Researches focusing on different morphologies, ranging from 0D Si particles, to 3D Si structures, have been reviewed, with special focuses on lithiation mechanism, advantages over bulk Si, and synthetic routes of various Si morphologies. Both physical and chemical methods have been commonly used for the preparation of Si nanostructures, including ball milling, sputtering deposition, PVD/CVD, chemical/electrochemical etching, reduction of silica. With that covered, some special attention is given to the recent effort micrometer-sized Si, which can be of more commercial interest. In general, there are two methodologies for the design of micrometer-sized Si with improved cycling performance in a LIB. One is the engineering of 3D structures of Si, with nanofeatures. The other strategy is to incorporate nano-sized Si onto a micrometer-sized host, such as graphite, and various carbon frameworks.

Long cycle life and good rate performance of Si-based anodes are usually more frequently observed with composites derived from nanostructured Si. This section of the review is more focused on the concepts and methods involved in the preparation of these composites, their physical properties and electrochemical performance. Carbon has been most widely adopted in the construction of Si-based composites, from simple carbon coating or mixing with Si, to the core–shell/yolk–shell structure construction, combination with graphene and CNT, hierarchical or 3D Si-C structures, etc. Conductive polymers, metal oxides, and some other noncarbonaceous materials have been adopted in Si composites. Other than the study on Si morphologies and development of various Si-based composites, there has been emerging research interest on auxiliary elements in a battery, such as electrolyte cosolvents, electrolyte additives, and functional binders, which play a unique role in creating a stable SEI layer, and helping maintain the electrode structure and conductivity. Despite the fact that nano-Si is more favorable in delivering high specific capacity and stable cycle performance, it is important to bear in mind the nanoapproach is not a panacea, and the ultimate target of the research on Si anodes is to obtain commercially competitive anodes, considering all practical aspects. While the problems associated with Si anodes cannot be fully solved with a single approach, a proper combination of the afore-mentioned strategies is highly desirable to achieve overall satisfactory performance and can be the key to the extensive commercialization of Si-based LIBs.

Supporting Information

Supporting Information is available from the Wiley Online Library or from the author.

Acknowledgements

This work was partially supported by NSERC and General Motors Global Research and Development Center. This work was also supported by the Assistant Secretary for Energy Efficiency and Renewable Energy, Office of Vehicle Technologies of the U.S. Department of Energy under Contract No. DE-AC02-05CH11231, Subcontract No. 7056410 under the Batteries for Advanced Transportation Technologies (BATT) Program.

Conflict of Interest

The authors declare no conflict of interest.

Keywords

binders, electrode engineering, electrolytes, lithium-ion batteries, silicon anodes

Received: August 8, 2017
Revised: October 10, 2017
Published online:

[1] M. T. McDowell, S. W. Lee, W. D. Nix, Y. Cui, *Adv. Mater.* **2013**, *25*, 4966.
[2] X. H. Liu, J. W. Wang, S. Huang, F. Fan, X. Huang, Y. Liu, S. Krylyuk, J. Yoo, S. A. Dayeh, A. V. Davydov, S. X. Mao, S. T. Picraux, S. Zhang, J. Li, T. Zhu, J. Y. Huang, *Nat. Nano* **2012**, *7*, 749.
[3] A. Bordes, E. De Vito, C. Haon, A. Boulineau, A. Montani, P. Marcus, *Chem. Mater.* **2016**. *28*, 1566.
[4] B. Key, R. Bhattacharyya, M. Morcrette, V. Seznec, J. M. Tarascon, C. P. Grey, *J. Am. Chem. Soc.* **2009**, *131*, 9239.
[5] B. Breitung, P. Baumann, H. Sommer, J. Janek, T. Brezesinski, *Nanoscale* **2016**, *8*, 14048.
[6] C. Y. Chen, T. Sano, T. Tsuda, K. Ui, Y. Oshima, M. Yamagata, M. Ishikawa, M. Haruta, T. Doi, M. Inaba, S. Kuwabata, *Sci. Rep.* **2016**, *6*, 36153.
[7] J. H. Ryu, J. W. Kim, Y. E. Sung, S. M. Oh, *Electrochem. Solid-State Lett.* **2004**, *7*, A306.
[8] F. Shi, Z. Song, P. N. Ross, G. A. Somorjai, R. O. Ritchie, K. Komvopoulos, *Nat. Commun.* **2016**, *7*, 11886.
[9] H. Wu, G. Chan, J. W. Choi, I. Ryu, Y. Yao, M. T. McDowell, S. W. Lee, A. Jackson, Y. Yang, L. B. Hu, Y. Cui, *Nat. Nanotechnol.* **2012**, *7*, 309.
[10] H. Wu, G. Y. Zheng, N. A. Liu, T. J. Carney, Y. Yang, Y. Cui, *Nano Lett.* **2012**, *12*, 904.

[11] Y. C. Yen, S. C. Chao, H. C. Wu, N. L. Wu, *J. Electrochem. Soc.* **2009**, *156*, A95.
[12] Y. Wen, Y. J. Zhu, A. Langrock, A. Manivannan, S. H. Ehrman, C. S. Wang, *Small* **2013**, *9*, 2810.
[13] E. Roduner, *Chem. Soc. Rev.* **2006**, *35*, 583.
[14] A. S. Arico, P. Bruce, B. Scrosati, J. M. Tarascon, W. van Schalk wijk, *Nat. Mater.* **2005**, *4*, 366.
[15] L. Y. Beaulieu, K. W. Eberman, R. L. Turner, L. J. Krause, J. R. Dahn, *Electrochem. Solid-State Lett.* **2001**, *4*, A137.
[16] L. Y. Beaulieu, T. D. Hatchard, A. Bonakdarpour, M. D. Fleischauer, J. R. Dahn, *J. Electrochem. Soc.* **2003**, *150*, A1457.
[17] H. Li, Z. X. Wang, L. Q. Chen, X. J. Huang, *Adv. Mater.* **2009**, *21*, 4593.
[18] W. Chen, Z. L. Fan, A. Dhanabalan, C. H. Chen, C. L. Wang, *J. Electrochem. Soc.* **2011**, *158*, A1055.
[19] Y. Yao, M. T. McDowell, I. Ryu, H. Wu, N. A. Liu, L. B. Hu, W. D. Nix, Y. Cui, *Nano Lett.* **2011**, *11*, 2949.
[20] M. Y. Ge, J. P. Rong, X. Fang, A. Y. Zhang, Y. H. Lu, C. W. Zhou, *Nano Res.* **2013**, *6*, 174.
[21] Q. Xiao, M. Gu, H. Yang, B. Li, C. Zhang, Y. Liu, F. Liu, F. Dai, L. Yang, Z. Liu, X. Xiao, G. Liu, P. Zhao, S. Zhang, C. Wang, Y. Lu, M. Cai, *Nat. Commun.* **2015**, *6*, 8844.
[22] H. T. Nguyen, F. Yao, M. R. Zamfir, C. Biswas, K. P. So, Y. H. Lee, S. M. Kim, S. N. Cha, J. M. Kim, D. Pribat, *Adv. Energy Mater.* **2011**, *1*, 1154.
[23] B. Laik, L. Eude, J. P. Pereira-Ramos, C. S. Cojocaru, D. Pribat, E. Rouviere, *Electrochim. Acta* **2008**, *53*, 5528.
[24] a) P. Das Kanungo, N. Zakharov, J. Bauer, O. Breitenstein, P. Werner, U. Goesele, *Appl. Phys. Lett.* **2008**, *92*, 3107; b) Y. H. Yang, S. J. Wu, H. S. Chin, P. I. Lin, Y. T. Chen, *J. Phys. Chem. B* **2004**, *108*, 846; c) Z. W. Pan, Z. R. Dai, L. Xu, S. T. Lee, Z. L. Wang, *J. Phys. Chem. B* **2001**, *105*, 2507.
[25] G. W. Zhou, H. Li, H. P. Sun, D. P. Yu, Y. Q. Wang, X. J. Huang, L. Q. Chen, Z. Zhang, *Appl. Phys. Lett.* **1999**, *75*, 2447.
[26] H. Li, X. J. Huang, L. Q. Chen, G. W. Zhou, Z. Zhang, D. P. Yu, Y. J. Mo, N. Pei, *Solid State Ionics* **2000**, *135*, 181.
[27] B. Gao, S. Sinha, L. Fleming, O. Zhou, *Adv. Mater.* **2001**, *13*, 816.
[28] C. K. Chan, H. L. Peng, G. Liu, K. McIlwrath, X. F. Zhang, R. A. Huggins, Y. Cui, *Nat. Nanotechnol.* **2008**, *3*, 31.
[29] T. D. Hatchard, J. R. Dahn, *J. Electrochem. Soc.* **2004**, *151*, A838.
[30] a) X. H. Liu, H. Zheng, L. Zhong, S. Huan, K. Karki, L. Q. Zhang, Y. Liu, A. Kushima, W. T. Liang, J. W. Wang, J. H. Cho, E. Epstein, S. A. Dayeh, S. T. Picraux, T. Zhu, J. Li, J. P. Sullivan, J. Cumings, C. S. Wang, S. X. Mao, Z. Z. Ye, S. L. Zhang, J. Y. Huang, *Nano Lett.* **2011**, *11*, 3312; b) H. Yang, S. Huang, X. Huang, F. F. Fan, W. T. Liang, X. H. Liu, L. Q. Chen, J. Y. Huang, J. Li, T. Zhu, S. L. Zhang, *Nano Lett.* **2012**, *12*, 1953; c) L. Luo, H. Yang, P. Yan, J. J. Travis, Y. Lee, N. Liu, D. Molina Piper, S.-H. Lee, P. Zhao, S. M. George, J.-G. Zhang, Y. Cui, S. Zhang, C. Ban, C.-M. Wang, *ACS Nano* **2015**, *9*, 5559; d) M. Y. Ge, J. P. Rong, X. Fang, C. W. Zhou, *Nano Lett.* **2012**, *12*, 2318; e) C. K. Chan, R. N. Patel, M. J. O'Connell, B. A. Korgel, Y. Cui, *ACS Nano* **2010**, *4*, 1443.
[31] Z. J. Du, S. C. Zhang, Y. Liu, J. F. Zhao, R. X. Lin, T. Jiang, *J. Mater. Chem.* **2012**, *22*, 11636.
[32] Z. Favors, H. H. Bay, Z. Mutlu, K. Ahmed, R. Ionescu, R. Ye, M. Ozkan, C. S. Ozkan, *Sci. Rep.* **2015**, *5*, 8246.
[33] D. J. Lee, H. Lee, M. H. Ryou, G. B. Han, J. N. Lee, J. Song, J. Choi, K. Y. Cho, Y. M. Lee, J. K. Park, *ACS Appl. Mater. Interfaces* **2013**, *5*, 12005.
[34] Q. Z. Xiao, Q. Zhang, Y. Fan, X. H. Wang, R. A. Susantyoko, *Energy Environ. Sci.* **2014**, *7*, 2261.
[35] T. Song, J. L. Xia, J. H. Lee, D. H. Lee, M. S. Kwon, J. M. Choi, J. Wu, S. K. Doo, H. Chang, W. Il Park, D. S. Zang, H. Kim, Y. G. Huang, K. C. Hwang, J. A. Rogers, U. Paik, *Nano Lett.* **2010**, *10*, 1710.
[36] a) Z. H. Wen, G. H. Lu, S. Mao, H. Kim, S. M. Cui, K. H. Yu, X. K. Huang, P. T. Hurley, O. Mao, J. H. Chen, *Electrochem. Commun.* **2013**, *29*, 67; b) Z. Z. Lu, T. L. Wong, T. W. Ng, C. D. Wang, *RSC Adv.* **2014**, *4*, 2440.
[37] M. H. Park, M. G. Kim, J. Joo, K. Kim, J. Kim, S. Ahn, Y. Cui, J. Cho, *Nano Lett.* **2009**, *9*, 3844.
[38] V. L. Chevrier, J. R. Dahn, *J. Electrochem. Soc.* **2009**, *156*, A454.
[39] J. R. Szczech, S. Jin, *Energy Environ. Sci.* **2011**, *4*, 56.
[40] S. Ohara, J. Suzuki, K. Sekine, T. Takamura, *J. Power Sources* **2004**, *136*, 303.
[41] a) J. Graetz, C. C. Ahn, R. Yazami, B. Fultz, *Electrochem. Solid-State Lett.* **2003**, *6*, A194; b) H. J. Jung, M. Park, S. H. Han, H. Lim, S. K. Joo, *Solid State Commun.* **2003**, *125*, 387; c) H. J. Jung, M. Park, Y. G. Yoon, G. B. Kim, S. K. Joo, *J. Power Sources* **2003**, *115*, 346.
[42] X. Su, Q. L. Wu, J. C. Li, X. C. Xiao, A. Lott, W. Q. Lu, B. W. Sheldon, J. Wu, *Adv. Energy Mater.* **2014**, *4*, 1300882.
[43] F. Luo, B. N. Liu, J. Y. Zheng, G. Chu, K. F. Zhong, H. Li, X. J. Huang, L. Q. Chen, *J. Electrochem. Soc.* **2015**, *162*, A2509.
[44] a) W. R. Liu, Z. Z. Guo, W. S. Young, D. T. Shieh, H. C. Wu, M. H. Yang, N. L. Wu, *J. Power Sources* **2005**, *140*, 139; b) S. Bourderau, T. Brousse, D. M. Schleich, *J. Power Sources* **1999**, *81*, 233.
[45] a) Y. Yu, L. Gu, C. B. Zhu, S. Tsukimoto, P. A. van Aken, J. Maier, *Adv. Mater.* **2010**, *22*, 2247; b) R. Yi, F. Dai, M. L. Gordin, H. Sohn, D. H. Wang, *Adv. Energy Mater.* **2013**, *3*, 1507; c) R. Yi, J. T. Zai, F. Dai, M. L. Gordin, D. H. Wang, *Nano Energy* **2014**, *6*, 211; d) H. J. Tian, X. J. Tan, F. X. Xin, C. S. Wang, W. Q. Han, *Nano Energy* **2015**, *11*, 490.
[46] a) X. Y. Zhu, H. Chen, Y. H. Wang, L. H. Xia, Q. Q. Tan, H. Li, Z. Y. Zhong, F. B. Su, X. S. Zhao, *J. Mater. Chem. A* **2013**, *1*, 4483; b) B. R. Liu, P. Soares, C. Checkles, Y. Zhao, G. H. Yu, *Nano Lett.* **2013**, *13*, 3414; c) J. Yu, H. H. Zhan, Y. H. Wang, Z. L. I. Zhang, H. Chen, H. Li, Z. Y. Zhong, F. B. Su, *J. Power Sources* **2013**, *228*, 112.
[47] D. S. Jung, T. H. Hwang, S. B. Park, J. W. Choi, *Nano Lett.* **2013**, *13*, 2092.
[48] S. Q. Chen, P. T. Bao, X. D. Huang, B. Sun, G. X. Wang, *Nano Res.* **2014**, *7*, 85.
[49] H. Kim, B. Han, J. Choo, J. Cho, *Angew. Chem., Int. Ed.* **2008**, *47*, 10151.
[50] R. Yi, F. Dai, M. L. Gordin, S. R. Chen, D. H. Wang, *Adv. Energy Mater.* **2013**, *3*, 295.
[51] Y. N. Jo, Y. Kim, J. S. Kim, J. H. Song, K. J. Kim, C. Y. Kwag, D. J. Lee, C. W. Park, Y. J. Kim, *J. Power Sources* **2010**, *195*, 6031.
[52] M. Li, X. H. Hou, Y. J. Sha, J. Wang, S. J. Hu, X. Liu, Z. P. Shao, *J. Power Sources* **2014**, *248*, 721.
[53] J. H. Lee, W. J. Kim, J. Y. Kim, S. H. Lim, S. M. Lee, *J. Power Sources* **2008**, *176*, 353.
[54] M. Ko, S. Chae, J. Ma, N. Kim, H.-W. Lee, Y. Cui, J. Cho, *Nat. Energy* **2016**, *1*, 16113.
[55] A. Magasinski, P. Dixon, B. Hertzberg, A. Kvit, J. Ayala, G. Yushin, *Nat. Mater.* **2010**, *9*, 353.
[56] Q. Xu, J.-Y. Li, J.-K. Sun, Y.-X. Yin, L.-J. Wan, Y.-G. Guo, *Adv. Energy Mater.* **2016**, 1601481.
[57] N. Liu, Z. D. Lu, J. Zhao, M. T. McDowell, H. W. Lee, W. T. Zhao, Y. Cui, *Nat. Nanotechnol.* **2014**, *9*, 187.
[58] a) H. Kim, M. Seo, M. H. Park, J. Cho, *Angew. Chem., Int. Ed.* **2010**, *49*, 2146; b) D. Mazouzi, B. Lestriez, L. Roue, D. Guyomard, *Electrochem. Solid-State Lett.* **2009**, *12*, A215.
[59] H. Li, X. J. Huang, L. Q. Chen, Z. G. Wu, Y. Liang, *Electrochem. Solid-State Lett.* **1999**, *2*, 547.
[60] P. F. Gao, J. W. Fu, J. Yang, R. G. Lv, J. L. Wang, Y. N. Nuli, X. Z. Tang, *Phys. Chem. Chem. Phys.* **2009**, *11*, 11101.

[61] a) J. Yang, B. F. Wang, K. Wang, Y. Liu, J. Y. Xie, Z. S. Wen, *Electrochem. Solid-State Lett.* **2003**, *6*, A154; b) T. H. Hwang, Y. M. Lee, B. S. Kong, J. S. Seo, J. W. Choi, *Nano Lett.* **2012**, *12*, 802.
[62] a) Y. Q. Zhang, X. H. Xia, X. L. Wang, Y. J. Mai, S. J. Shi, Y. Y. Tang, L. Li, J. P. Tu, *Electrochem. Commun.* **2012**, *23*, 17; b) H. F. Xiang, K. Zhang, G. Ji, J. Y. Lee, C. J. Zou, X. D. Chen, J. S. Wu, *Carbon* **2011**, *49*, 1787.
[63] K. Evanoff, A. Magasinski, J. B. Yang, G. Yushin, *Adv. Energy Mater.* **2011**, *1*, 495.
[64] a) R. Epur, M. K. Datta, P. N. Kumta, *Electrochim. Acta* **2012**, *85*, 680; b) W. Wang, I. Ruiz, K. Ahmed, H. H. Bay, A. S. George, J. Wang, J. Butler, M. Ozkan, C. S. Ozkan, *Small* **2014**, *10*, 3389.
[65] W. Wang, P. N. Kumta, *ACS Nano* **2010**, *4*, 2233.
[66] Y. Chen, S. Zeng, J. F. Qian, Y. D. Wang, Y. L. Cao, H. X. Yang, X. P. Ai, *ACS Appl. Mater. Interfaces* **2014**, *6*, 3508.
[67] M. D. Fleischauer, M. N. Obrovac, J. R. Dahn, *J. Electrochem. Soc.* **2008**, *155*, A851.
[68] J. R. Dahn, R. E. Mar, M. D. Fleischauer, M. N. Obrovac, *J. Electrochem. Soc.* **2006**, *153*, A1211.
[69] a) M. S. Wang, W. L. Song, L. Z. Fan, *J. Mater. Chem. A* **2015**, *3*, 12709; b) B. Li, F. Yao, J. J. Bae, J. Chang, M. R. Zamfir, D. T. Le, D. T. Pham, H. Yue, Y. H. Lee, *Sci. Rep.* **2015**, *5*, 7659.
[70] a) Y. Liu, K. Hanai, J. Yang, N. Imanishi, A. Hirano, Y. Takeda, *Electrochem. Solid-State Lett.* **2004**, *7*, A369; b) Y. S. Hu, R. Demir-Cakan, M. M. Titirici, J. O. Muller, R. Schlogl, M. Antonietti, J. Maier, *Angew. Chem., Int. Ed.* **2008**, *47*, 1645.
[71] Q. Si, K. Hanai, N. Imanishi, M. Kubo, A. Hirano, Y. Takeda, O. Yamamoto, *J. Power Sources* **2009**, *189*, 761.
[72] Y. Liu, Z. Y. Wen, X. Y. Wang, A. Hirano, N. Imanishi, Y. Takeda, *J. Power Sources* **2009**, *189*, 733.
[73] Y. S. Jung, K. T. Lee, S. M. Oh, *Electrochim. Acta* **2007**, *52*, 7061.
[74] a) S. Li, X. Y. Qin, H. R. Zhang, J. X. Wu, Y. B. He, B. H. Li, F. Y. Kang, *Electrochem. Commun.* **2014**, *49*, 98; b) Y. H. Xu, G. P. Yin, Y. L. Ma, P. J. Zuo, X. Q. Cheng, *J. Mater. Chem.* **2010**, *20*, 3216.
[75] a) H. Kim, J. Cho, *Nano Lett.* **2008**, *8*, 3688; b) S. A. Klankowski, R. A. Rojeski, B. A. Cruden, J. W. Liu, J. Wu, J. Li, *J. Mater. Chem. A* **2013**, *1*, 1055; c) G. Jeong, J. G. Kim, M. S. Park, M. Seo, S. M. Hwang, Y. U. Kim, Y. J. Kim, J. H. Kim, S. X. Dou, *ACS Nano* **2014**, *8*, 2977.
[76] X. L. Li, P. Meduri, X. L. Chen, W. Qi, M. H. Engelhard, W. Xu, F. Ding, J. Xiao, W. Wang, C. M. Wang, J. G. Zhang, J. Liu, *J. Mater. Chem.* **2012**, *22*, 11014.
[77] J. P. Yang, Y. X. Wang, S. L. Chou, R. Y. Zhang, Y. F. Xu, J. W. Fan, W. X. Zhang, H. K. Liu, D. Y. Zhao, S. X. Dou, *Nano Energy* **2015**, *18*, 133.
[78] N. Liu, H. Wu, M. T. McDowell, Y. Yao, C. M. Wang, Y. Cui, *Nano Lett.* **2012**, *12*, 3315.
[79] X. C. Xiao, W. D. Zhou, Y. N. Kim, I. Ryu, M. Gu, C. M. Wang, G. Liu, Z. Y. Liu, H. J. Gao, *Adv. Funct. Mater.* **2015**, *25*, 1426.
[80] K. S. Novoselov, A. K. Geim, S. V. Morozov, D. Jiang, Y. Zhang, S. V. Dubonos, I. V. Grigorieva, A. A. Firsov, *Science* **2004**, *306*, 666.
[81] a) K. S. Novoselov, V. I. Fal'ko, L. Colombo, P. R. Gellert, M. G. Schwab, K. Kim, *Nature* **2012**, *490*, 192; b) S. Stankovich, D. A. Dikin, G. H. B. Dommett, K. M. Kohlhaas, E. J. Zimney, E. A. Stach, R. D. Piner, S. T. Nguyen, R. S. Ruoff, *Nature* **2006**, *442*, 282; c) F. Bonaccorso, L. Colombo, G. Yu, M. Stoller, V. Tozzini, A. C. Ferrari, R. S. Ruoff, V. Pellegrini, *Science* **2015**, *347*, 6217.
[82] a) E. Yoo, J. Kim, E. Hosono, H. Zhou, T. Kudo, I. Honma, *Nano Lett.* **2008**, *8*, 2277; b) G. X. Wang, X. P. Shen, J. Yao, J. Park, *Carbon* **2009**, *47*, 2049; c) Z. S. Wu, W. C. Ren, L. Xu, F. Li, H. M. Cheng, *ACS Nano* **2011**, *5*, 5463; d) X. F. Li, D. S. Geng, Y. Zhang, X. B. Meng, R. Y. Li, X. L. Sun, *Electrochem. Commun.* **2011**, *13*, 822; e) H. F. Xiang, Z. D. Li, K. Xie, J. Z. Jiang, J. J. Chen, P. C. Lian, J. S. Wu, Y. Yu, H. H. Wang, *RSC Adv.* **2012**, *2*, 6792; f) P. C. Lian, X. F. Zhu, S. Z. Liang, Z. Li, W. S. Yang, H. H. Wang, *Electrochim. Acta* **2010**, *55*, 3909.
[83] a) D. H. Wang, D. W. Choi, J. Li, Z. G. Yang, Z. M. Nie, R. Kou, D. H. Hu, C. M. Wang, L. V. Saraf, J. G. Zhang, I. A. Aksay, J. Liu, *ACS Nano* **2009**, *3*, 907; b) B. Luo, Y. Fang, B. Wang, J. S. Zhou, H. H. Song, L. J. Zhi, *Energy Environ. Sci.* **2012**, *5*, 5226; c) N. Li, Z. P. Chen, W. C. Ren, F. Li, H. M. Cheng, *Proc. Natl. Acad. Sci. USA* **2012**, *109*, 17360.
[84] J. K. Lee, K. B. Smith, C. M. Hayner, H. H. Kung, *Chem. Commun.* **2010**, *46*, 2025.
[85] S. L. Chou, J. Z. Wang, M. Choucair, H. K. Liu, J. A. Stride, S. X. Dou, *Electrochem. Commun.* **2010**, *12*, 303.
[86] J. Z. Wang, C. Zhong, S. L. Chou, H. K. Liu, *Electrochem. Commun.* **2010**, *12*, 1467.
[87] W. S. Hummers, R. E. Offeman, *J. Am. Chem. Soc.* **1958**, *80*, 1339.
[88] a) X. S. Zhou, Y. X. Yin, L. J. Wan, Y. G. Guo, *Chem. Commun.* **2012**, *48*, 2198; b) V. Chabot, K. Feng, H. W. Park, F. M. Hassan, A. R. Elsayed, A. P. Yu, X. C. Xiao, Z. W. Chen, *Electrochim. Acta* **2014**, *130*, 127; c) J. Y. Luo, X. Zhao, J. S. Wu, H. D. Jang, H. H. Kung, J. X. Huang, *J. Phys. Chem. Lett.* **2012**, *3*, 1824; d) Y. Li, K. Yan, H.-W. Lee, Z. Lu, N. Liu, Y. Cui, *Nat. Energy* **2016**, *1*, 15029.
[89] a) X. S. Zhou, Y. X. Yin, L. J. Wan, Y. G. Guo, *Adv. Energy Mater.* **2012**, *2*, 1086; b) A. R. Park, J. S. Kim, K. S. Kim, K. Zhang, J. Park, J. H. Park, J. K. Lee, P. J. Yoo, *ACS Appl. Mater. Interfaces* **2014**, *6*, 1702; c) F. H. Du, K. X. Wang, W. Fu, P. F. Gao, J. F. Wang, J. Yang, J. S. Chen, *J. Mater. Chem. A* **2013**, *1*, 13648; d) H. Mi, F. Li, C. He, X. Chai, Q. Zhang, C. Li, Y. Li, J. Liu, *Electrochim. Acta* **2016**, *190*, 1032; e) Z. F. Li, H. Y. Zhang, Q. Liu, Y. D. Liu, L. Stanciu, J. Xie, *ACS Appl. Mater. Interfaces* **2014**, *6*, 5996.
[90] Y. L. Huang, X. H. Hou, X. Y. Fan, S. M. Ma, S. J. Hu, K. H. Lam, *Electrochim. Acta* **2015**, *182*, 1175.
[91] K. Feng, W. Ahn, G. Lui, H. W. Park, A. G. Kashkooli, G. Jiang, X. Wang, X. Xiao, Z. Chen, *Nano Energy* **2016**, *19*, 187.
[92] a) X. Liu, J. Zhang, W. Si, L. Xi, B. Eichler, C. Yan, O. G. Schmidt, *ACS Nano* **2015**, *9*, 1198; b) B. Wang, X. L. Li, X. F. Zhang, B. Luo, M. H. Jin, M. H. Liang, S. A. Dayeh, S. T. Picraux, L. J. Zhi, *ACS Nano* **2013**, *7*, 1437; c) M. Ko, S. Chae, S. Jeong, P. Oh, J. Cho, *ACS Nano* **2014**, *8*, 8591.
[93] B. Li, S. Yang, S. Li, B. Wang, J. Liu, *Adv. Energy Mater.* **2015**, 1500289.
[94] I. H. Son, J. Hwan Park, S. Kwon, S. Park, M. H. Rummeli, A. Bachmatiuk, H. J. Song, J. Ku, J. W. Choi, J.-m. Choi, S.-G. Doo, H. Chang, *Nat. Commun.* **2015**, *6*, 7393.
[95] H. W. Mi, Y. L. Li, P. Y. Zhu, X. Y. Chai, L. N. Sun, H. T. Zhuo, Q. L. Zhang, C. X. He, J. H. Liu, *J. Mater. Chem. A* **2014**, *2*, 11254.
[96] J. Y. Ji, H. X. Ji, L. L. Zhang, X. Zhao, X. Bai, X. B. Fan, F. B. Zhang, R. S. Ruoff, *Adv. Mater.* **2013**, *25*, 4673.
[97] F. M. Hassan, A. R. Elsayed, V. Chabot, R. Batmaz, X. C. Xiao, Z. W. Chen, *ACS Appl. Mater. Interfaces* **2014**, *6*, 13757.
[98] W. X. Zhang, Z. Z. Zhang, Y. G. Zhang, *Nanoscale Res. Lett.* **2011**, *6*, 555.
[99] a) A. C. Dillon, *Chem. Rev.* **2010**, *110*, 6856; b) M. W. Rowell, M. A. Topinka, M. D. McGehee, H. J. Prall, G. Dennler, N. S. Sariciftci, L. B. Hu, G. Gruner, *Appl. Phys. Lett.* **2006**, *88*, 233506; c) E. Frackowiak, F. Beguin, *Carbon* **2002**, *40*, 1775; d) Z. Chen, A. P. Yu, D. Higgins, H. Li, H. J. Wang, Z. W. Chen, *Nano Lett.* **2012**, *12*, 1946; e) Z. Chen, D. Higgins, Z. W. Chen, *Carbon* **2010**, *48*, 3057; f) Z. Chen, D. Higgins, H. S. Tao, R. S. Hsu, Z. W. Chen, *J. Phys. Chem. C* **2009**, *113*, 21008.
[100] a) M. S. Mauter, M. Elimelech, *Environ. Sci. Technol.* **2008**, *42*, 5843; b) C. W. Tan, K. H. Tan, Y. T. Ong, A. R. Mohamed, S. H. S. Zein, S. H. Tan, *Environ. Chem. Lett.* **2012**, *10*, 265.
[101] B. J. Landi, M. J. Ganter, C. D. Cress, R. A. DiLeo, R. P. Raffaelle, *Energy Environ. Sci.* **2009**, *2*, 638.

[102] B. J. Landi, C. M. Evans, J. J. Worman, S. L. Castro, S. G. Bailey, R. P. Raffaelle, *Mater. Lett.* **2006**, *60*, 3502.
[103] Y. Zhang, X. G. Zhang, H. L. Zhang, Z. G. Zhao, F. Li, C. Liu, H. M. Cheng, *Electrochim. Acta* **2006**, *51*, 4994.
[104] J. Shu, H. Li, R. Z. Yang, Y. Shi, X. J. Huang, *Electrochem. Commun.* **2006**, *8*, 51.
[105] a) J. Bae, *J. Solid State Chem.* **2011**, *184*, 1749; b) K. Goldshtein, K. Freedman, D. Schneier, L. Burstein, V. Ezersky, E. Peled, D. Golodnitsky, *J. Electrochem. Soc.* **2015**, *162*, A1072; c) D. Lin, Z. Lu, P.-C. Hsu, H. R. Lee, N. Liu, J. Zhao, H. Wang, C. Liu, Y. Cui, *Energy Environ. Sci.* **2015**, *8*, 2371.
[106] M. W. Forney, M. J. Ganter, J. W. Staub, R. D. Ridgley, B. J. Landi, *Nano Lett.* **2013**, *13*, 4158.
[107] M. S. Park, S. Rajendran, Y. M. Kang, K. S. Han, Y. S. Han, J. Y. Lee, *J. Power Sources* **2006**, *158*, 650.
[108] Y. Fan, Q. Zhang, Q. Z. Xiao, X. H. Wang, K. Huang, *Carbon* **2013**, *59*, 264.
[109] H. Y. Lin, C. H. Li, D. Y. Wang, C. C. Chen, *Nanoscale* **2016**, *8*, 1280.
[110] F.-H. Du, B. Li, W. Fu, Y.-J. Xiong, K.-X. Wang, J.-S. Chen, *Adv. Mater.* **2014**, *26*, 6145.
[111] H. Wu, G. H. Yu, L. J. Pan, N. A. Liu, M. T. McDowell, Z. A. Bao, Y. Cui, *Nat. Commun.* **2013**, *4*, 1943.
[112] P. R. Abel, A. M. Chockla, Y. M. Lin, V. C. Holmberg, J. T. Harris, B. A. Korgel, A. Heller, C. B. Mullins, *ACS Nano* **2013**, *7*, 2249.
[113] L. Y. Beaulieu, K. C. Hewitt, R. L. Turner, A. Bonakdarpour, A. A. Abdo, L. Christensen, K. W. Eberman, J. L. Krause, J. R. Dahn, *J. Electrochem. Soc.* **2003**, *150*, A149.
[114] L. Christensen, M. N. Obrovac, *US Patent 7732095 B2* **2010**.
[115] J. I. Lee, Y. Ko, M. Shin, H. K. Song, N. S. Choi, M. G. Kim, S. Park, *Energy Environ. Sci.* **2015**, *8*, 2075.
[116] a) M. K. Wang, L. Qi, F. Zhao, S. J. Dong, *J. Power Sources* **2005**, *139*, 223; b) J. M. Tarascon, M. Armand, *Nature* **2001**, *414*, 359.
[117] a) B. Philippe, R. Dedryvere, J. Allouche, F. Lindgren, M. Gorgoi, H. Rensmo, D. Gonbeau, K. Edstrom, *Chem. Mater.* **2012**, *24*, 1107; b) A. M. Andersson, K. Edstrom, *J. Electrochem. Soc.* **2001**, *148*, A1100.
[118] a) L. Pan, H. B. Wang, D. C. Gao, S. Y. Chen, L. Tan, L. Li, *Chem. Commun.* **2014**, *50*, 5878; b) S. D. Beattie, D. Larcher, M. Morcrette, B. Simon, J. M. Tarascon, *J. Electrochem. Soc.* **2008**, *155*, A158; c) M. Holzapfel, H. Buqa, L. J. Hardwick, M. Hahn, A. Wursig, W. Scheifele, P. Novak, R. Kotz, C. Veit, F. M. Petrat, *Electrochim. Acta* **2006**, *52*, 973.
[119] G. B. Han, M. H. Ryou, K. Y. Cho, Y. M. Lee, J. K. Park, *J. Power Sources* **2010**, *195*, 3709.
[120] S. Y. Li, B. C. Li, X. L. Xu, X. M. Shi, Y. Y. Zhao, L. P. Mao, X. L. Cui, *J. Power Sources* **2012**, *209*, 295.
[121] S. Dalavi, P. Guduru, B. L. Lucht, *J. Electrochem. Soc.* **2012**, *159*, A642.
[122] L. B. Chen, K. Wang, X. H. Xie, J. Y. Xie, *J. Power Sources* **2007**, *174*, 538.
[123] Y. M. Lin, K. C. Klavetter, P. R. Abel, N. C. Davy, J. L. Snider, A. Heller, C. B. Mullins, *Chem. Commun.* **2012**, *48*, 7268.
[124] V. Etacheri, O. Haik, Y. Goffer, G. A. Roberts, I. C. Stefan, R. Fasching, D. Aurbach, *Langmuir* **2012**, *28*, 965.
[125] a) M. Gauthier, T. J. Carney, A. Grimaud, L. Giordano, N. Pour, H. H. Chang, D. P. Fenning, S. F. Lux, O. Paschos, C. Bauer, F. Magia, S. Lupart, P. Lamp, Y. Shao-Horn, *J. Phys. Chem. Lett.* **2015**, *6*, 4653; b) H. Zhao, S. J. Park, F. F. Shi, Y. B. Fu, V. Battaglia, P. N. Ross, G. Liu, *J. Electrochem. Soc.* **2014**, *161*, A194.
[126] K. Xu, *Chem. Rev.* **2014**, *114*, 11503.
[127] H. Ota, Y. Sakata, A. Inoue, S. Yamaguchi, *J. Electrochem. Soc.* **2004**, *151*, A1659.
[128] M. C. Smart, B. V. Ratnakumar, L. D. Whitcanack, K. B. Chin, S. Surampudi, H. Croft, D. Tice, R. Staniewicz, *J. Power Sources* **2003**, *119*, 349.
[129] H. Nakai, T. Kubota, A. Kita, A. Kawashima, *J. Electrochem. Soc.* **2011**, *158*, A798.
[130] C. Xu, F. Lindgren, B. Philippe, M. Gorgoi, F. Bjorefors, K. Edstrom, T. Gustafsson, *Chem. Mater.* **2015**, *27*, 2591.
[131] S. Malmgren, K. Ciosek, M. Hahlin, T. Gustafsson, M. Gorgoi, H. Rensmo, K. Edstrom, *Electrochim. Acta* **2013**, *97*, 23.
[132] K. Schroder, J. Avarado, T. A. Yersak, J. C. Li, N. Dudney, L. J. Webb, Y. S. Meng, K. J. Stevenson, *Chem. Mater.* **2015**, *27*, 5531.
[133] C. C. Nguyen, B. L. Lucht, *J. Electrochem. Soc.* **2014**, *161*, A1933.
[134] J. M. M. de la Hoz, P. B. Balbuena, *Phys. Chem. Chem. Phys.* **2014**, *16*, 17091.
[135] M. Ulldemolins, F. Le Cras, B. Pecquenard, V. P. Phan, L. Martin, H. Martinez, *J. Power Sources* **2012**, *206*, 245.
[136] I. A. Profatilova, C. Stock, A. Schmitz, S. Passerini, M. Winter, *J. Power Sources* **2013**, *222*, 140.
[137] M. Q. Li, M. Z. Qu, X. Y. He, Z. L. Yu, *Electrochim. Acta* **2009**, *54*, 4506.
[138] S. J. Lee, J. G. Han, Y. Lee, M. H. Jeong, W. C. Shin, M. Ue, N. S. Choi, *Electrochim. Acta* **2014**, *137*, 1.
[139] W. R. Liu, M. H. Yang, H. C. Wu, S. M. Chiao, N. L. Wu, *Electrochem. Solid-State Lett.* **2005**, *8*, A100.
[140] E. Markevich, G. Salitra, D. Aurbach, *Electrochem. Commun.* **2005**, *7*, 1298.
[141] Y. K. Jeong, T. W. Kwon, I. Lee, T. S. Kim, A. Coskun, J. W. Choi, *Nano Lett.* **2014**, *14*, 864.
[142] J. X. Song, M. J. Zhou, R. Yi, T. Xu, M. L. Gordin, D. H. Tang, Z. X. Yu, M. Regula, D. H. Wang, *Adv. Funct. Mater.* **2014**, *24*, 5904.
[143] B. Koo, H. Kim, Y. Cho, K. T. Lee, N. S. Choi, J. Cho, *Angew. Chem., Int. Ed.* **2012**, *51*, 8762.
[144] Y. K. Jeong, T. W. Kwon, I. Lee, T. S. Kim, A. Coskun, J. W. Choi, *Energy Environ. Sci.* **2015**, *8*, 1224.
[145] A. Magasinski, B. Zdyrko, I. Kovalenko, B. Hertzberg, R. Burtovyy, C. F. Huebner, T. F. Fuller, I. Luzinov, G. Yushin, *ACS Appl. Mater. Interfaces* **2010**, *2*, 3004.
[146] C. Chen, S. H. Lee, M. Cho, J. Kim, Y. Lee, *ACS Appl. Mater. Interfaces* **2016**, *8*, 2658.
[147] C. Wang, H. Wu, Z. Chen, M. T. McDowell, Y. Cui, Z. A. Bao, *Nat. Chem.* **2013**, *5*, 1043.
[148] C. C. Nguyen, T. Yoon, D. M. Seo, P. Guduru, B. L. Lucht, *ACS Appl. Mater. Interfaces* **2016**, *8*, 12211.
[149] M. Y. Wu, X. Y. Song, X. S. Liu, V. Battaglia, W. L. Yang, G. Liu, *J. Mater. Chem. A* **2015**, *3*, 3651.
[150] M. Y. Wu, X. C. Xiao, N. Vukmirovic, S. D. Xun, P. K. Das, X. Y. Song, P. Olalde-Velasco, D. D. Wang, A. Z. Weber, L. W. Wang, V. S. Battaglia, W. L. Yang, G. Liu, *J. Am. Chem. Soc.* **2013**, *135*, 12048.
[151] W. R. Liu, J. H. Wang, H. C. Wu, D. T. Shieh, M. H. Yang, N. L. Wu, *J. Electrochem. Soc.* **2005**, *152*, A1719.
[152] T. M. Higgins, S. H. Park, P. J. King, C. Zhang, N. McEvoy, N. C. Berner, D. Daly, A. Shmeliov, U. Khan, G. Duesberg, V. Nicolosi, J. N. Coleman, *ACS Nano* **2016**, *10*, 3702.
[153] G. Liu, S. D. Xun, N. Vukmirovic, X. Y. Song, P. Olalde-Velasco, H. H. Zheng, V. S. Battaglia, L. W. Wang, W. L. Yang, *Adv. Mater.* **2011**, *23*, 4679.
[154] L. F. Cui, L. B. Hu, H. Wu, J. W. Choi, Y. Cui, *J. Electrochem. Soc.* **2011**, *158*, A592.
[155] H. Zhao, Y. Wei, R. M. Qiao, C. H. Zhu, Z. Y. Zheng, M. Ling, Z. Jia, Y. Bai, Y. B. Fu, J. L. Lei, X. Y. Song, V. S. Battaglia, W. L. Yang, P. B. Messersmith, G. Liu, *Nano Lett.* **2015**, *15*, 7927.
[156] a) E. Peled, F. Patolsky, D. Golodnitsky, K. Freedman, G. Davidi, D. Schneier, *Nano Lett.* **2015**, *15*, 3907; b) X. L. Li, J. H. Cho, N. Li, Y. Y. Zhang, D. Williams, S. A. Dayeh, S. T. Picraux, *Adv. Energy Mater.* **2012**, *2*, 87; c) J. Liu, N. Li, M. D. Goodman, H. G. Zhang, E. S. Epstein, B. Huang, Z. Pan, J. Kim, J. H. Choi, X. Huang, J. Liu, K. J. Hsia, S. J. Dillon, P. V. Braun, *ACS Nano* **2015**, *9*, 1985.

[157] a) X. H. Yu, H. Y. Yang, H. W. Meng, Y. L. Sun, J. Zheng, D. Q. Ma, X. H. Xu, *ACS Appl. Mater. Interfaces* **2015**, *7*, 15961; b) S. J. Park, H. Zhao, G. Ai, C. Wang, X. Y. Song, N. Yuca, V. S. Battaglia, W. L. Yang, G. Liu, *J. Am. Chem. Soc.* **2015**, *137*, 2565.
[158] T. R. Jow, L. W. Shacklette, *J. Electrochem. Soc.* **1988**, *135*, 541.
[159] L. F. Cui, R. Ruffo, C. K. Chan, H. L. Peng, Y. Cui, *Nano Lett.* **2009**, *9*, 491.
[160] B. Liu, X. F. Wang, H. T. Chen, Z. R. Wang, D. Chen, Y. B. Cheng, C. W. Zhou, G. Z. Shen, *Sci. Rep.* **2013**, *3*, 1622.
[161] F. M. Hassan, V. Chabot, A. R. Elsayed, X. C. Xiao, Z. W. Chen, *Nano Lett.* **2014**, *14*, 277.
[162] F. M. Hassan, R. Batmaz, J. D. Li, X. L. Wang, X. C. Xiao, A. P. Yu, Z. W. Chen, *Nat. Commun.* **2015**, *6*, 8597.
[163] L. F. Cui, Y. Yang, C. M. Hsu, Y. Cui, *Nano Lett.* **2009**, *9*, 3370.
[164] P. P. Prosini, C. Cento, A. Rufoloni, F. Rondino, A. Santoni, *Solid State Ionics* **2015**, *269*, 93.
[165] W. Sun, R. Z. Hu, H. Liu, M. Q. Zeng, L. C. Yang, H. H. Wang, M. Zhu, *J. Power Sources* **2014**, *268*, 610.
[166] L. W. Ji, H. H. Zheng, A. Ismach, Z. K. Tan, S. D. Xun, E. Lin, V. Battaglia, V. Srinivasan, Y. G. Zhang, *Nano Energy* **2012**, *1*, 164.
[167] M. A. Pope, I. A. Aksay, *Adv. Energy. Mater.* **2015**, *5*, 1500124.
[168] a) J. Hassoun, J. Kim, D. J. Lee, H. G. Jung, S. M. Lee, Y. K. Sun, B. Scrosati, *J. Power Sources* **2012**, *202*, 308; b) M. Agostini, J. Hassoun, J. Liu, M. Jeong, H. Nara, T. Momma, T. Osaka, Y. K. Sun, B. Scrosati, *ACS Appl. Mater. Interfaces* **2014**, *6*, 10924.
[169] S. K. Lee, S. M. Oh, E. Park, B. Scrosati, J. Hassoun, M. S. Park, Y. J. Kim, H. Kim, I. Belharouak, Y. K. Sun, *Nano Lett.* **2015**, *15*, 2863.
[170] a) X. Pu, G. Yang, C. H. Yu, *Nano Energy* **2014**, *9*, 318; b) Y. Yan, Y. X. Yin, S. Xin, J. Su, Y. G. Guo, L. J. Wan, *Electrochim. Acta* **2013**, *91*, 58.
[171] C. F. Shen, M. Y. Ge, A. Y. Zhang, X. Fang, Y. H. Liu, J. P. Rong, C. W. Zhou, *Nano Energy* **2016**, *19*, 68.
[172] Y. Yang, M. T. McDowell, A. Jackson, J. J. Cha, S. S. Hong, Y. Cui, *Nano Lett.* **2010**, *10*, 1486.
[173] a) H. Jha, I. Buchberger, X. Y. Cui, S. Meini, H. A. Gasteiger, *J. Electrochem. Soc.* **2015**, *162*, A1829; b) M. Wenberger, M. Wohlfahrt-Mehrens, *Electrochim. Acta* **2016**, *191*, 124.
[174] T. Yim, M. S. Park, J. S. Yu, K. J. Kim, K. Y. Im, J. H. Kim, G. Jeong, Y. N. Jo, S. G. Woo, K. S. Kang, I. Lee, Y. J. Kim, *Electrochim. Acta* **2013**, *107*, 454.
[175] B. Li, S. M. Li, J. J. Xu, S. B. Yang, *Energy Environ. Sci.* **2016**, *9*, 2025.